Journal of Nanobiotechnology

REVIEW

Open Access

The develop of persistent luminescence nanoparticles with excellent performances in cancer targeted bioimaging and killing: a review

Rongshuang Tan[1†], Jianing Wu[1†], Chunya Wang[1], Zhengyan Zhao[1], Xiaoyuan Zhang[1], Chang Zhong[1], Zihui Tang[1], Rui Zheng[1], Binhong Du[2], Yunhan He[1], Yuhua Sun[3,4*] and Ping Zhou[1*]

Abstract

The use of fluorescent nanomaterials in tumor imaging and treatment effectively avoids the original limitations of traditional tumor clinical diagnostic methods. The PLNPs emitted persistent luminescence after the end of excitation light. Owing to their superior optical properties, such as a reduced laser irradiation dose, spontaneous fluorescence interference elimination, and near-infrared imaging, PLNPs show great promise in tumor imaging. Moreover, they also achieve excellent anti-tumor therapeutic effects through surface modification and drug delivery. However, their relatively large size and limited surface modification capacity limit their ability to kill tumors effectively enough for clinical applications. Thus, this article reviews the synthesis and modification of PLNPs and the research progress in targeted tumor imaging and tumor killing. We also discuss the challenges and prospects of their future applications in these fields. This review has value for accelerating the design of PLNPs based platform for cancer diagnosis and treatment.

Keywords Persistent luminescence nanoparticles, Cancer treatment, Bioimaging, Tumor monitoring, Cell killing

[†]Rongshuang Tan and Jianing Wu have contributed equally to this work.

*Correspondence:
Yuhua Sun
yuhua-sun@xzhmu.edu.cn
Ping Zhou
zhoup@lzu.edu.cn
Full list of author information is available at the end of the article

Graphical abstract

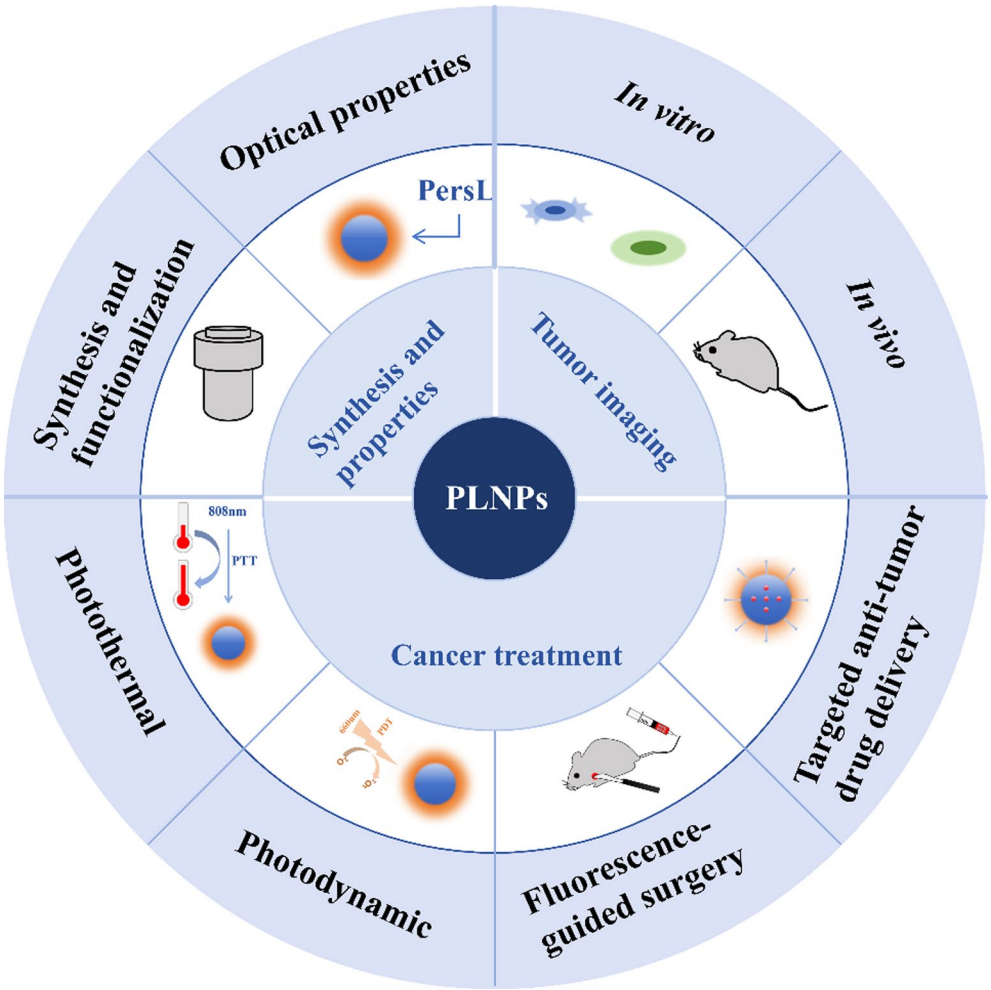

Introduction

Because of the increasing cancer incidence worldwide, the realization of accurate diagnosis and treatment of cancer needs extensive research [1–4]. The difficulty lies in how to accurately distinguish between normal cells and tumor cells. Traditional clinical methods include computed tomography (CT), positron emission tomography (PET) and magnetic resonance imaging (MRI) [5–7]. Among them, CT has the advantages of good resolution, but its limitation lies in radiation problems and high cost [8]. The safety of MRI is a considerable advantage, but the lack of sensitivity and artifacts caused by motion are its disadvantages [9]. PET shows higher sensitivity and quantitative detection than both methods do, but the problems of cost and limited instruments need to be solved [10]. In this context, fluorescence imaging technology enables tumor monitoring and real-time guidance during surgery with ideal imaging effect, which reduces ionizing radiation and radiation damage and is helpful for overcoming the problems of high technical cost and limited instrument use, especially in terms of sensitivity and specificity at the cellular level [11, 12]. To date, a variety of fluorescent nanomaterials have been applied in fields such as biological imaging, tumor diagnosis and tumor treatment [13–15]. Traditional agents, including porphyrins, phthalocyanines and other organic dyes, are limited by easy photobleaching and long-term photoactivation [16–18]. Thus, novel fluorescent nanomaterials of carbon quantum dots and gold nanorods with sufficient optical stability have been developed for anti-tumor treatment [19, 20]. However, their limited luminescence time makes eliminating the interference of

spontaneous fluorescence background in practical applications difficult, which limits the further application of long-term and real-time imaging [21]. Fortunately, persistent luminescence nanoparticles (PLNPs), which can store the energy generated by the excitation source and continue to release the energy gradually after the excitation has stopped, show great promise for application as fluorescent probes for biological imaging [22]. The application of PLNPs can reduce the laser irradiation dose and eliminate the interference of real-time excitation from external light sources, which is conducive to achieving safer and more sensitive long-term in vivo imaging [23–25]. In addition, the emergence of near-infrared (NIR)-emitting PLNPs further enhances the in vivo penetration depth of fluorescent probes, indicating extremely ideal clinical and research application prospects in tumor cell killing [26, 27].

At present, although some PLNPs based materials have been reported for tumor diagnosis and treatment, a comprehensive review related to anti-tumor applications is still relatively lacking. Moreover, there is no systematic explanation for the shortcomings of PLNPs in tumor diagnosis and treatment research, including the need for nanometer-scale PLNPs, further improvement in tumor killing efficiency, and consideration of their combination with other bioimaging methods. Therefore, this review summarizes the development status of the preparation methods, optical properties and biocompatibility of PLNPs, with a focus on related applications in tumor imaging and treatment through modifications and drug delivery, including photothermal therapy (PTT), photodynamic therapy (PDT), guided surgery-targeted antitumor drug delivery treatment and fluorescence-guided surgery. We also discuss corresponding prospects, aiming to provide a systematic viewpoint and propose new ideas for related research. Our work provides necessary theoretical support and new research directions for further studies of the anti-tumor applications of PLNPs.

Synthesis methods and surface functionalization of PLNPs

Synthesis methods of PLNPs

Conventional persistent phosphors are synthesized by high-temperature solid-state reactions using powdered raw materials. This traditional method has the advantages of high crystallinity, strong luminescence and a long afterglow time. However, owing to the uncontrollability of mechanical grinding during the synthesis process, the particle size is usually approximately tens of micrometers with uneven size and irregular morphology, which is not conducive to its wide application in biomedical fields [28].

The synthesis of PLNPs with a uniform and regular morphology is essential for the application of persistent phosphors in biomedical fields, especially in medical oncology [29]. These properties help to improve the quality and sensitivity of tumor imaging, and PLNPs with homogeneous sizes and regular morphologies are more conducive to surface functionalization to construct PLNPs for diagnostic and therapeutic integrated nanoplatforms. Thus, there is an urgent need for researchers to explore new synthesis methods to obtain PLNPs. To overcome the drawbacks of traditional synthesis methods, many studies have been conducted for this purpose. In recent years, the emergence of so-called "bottom-up" nanoscale synthesis methods, including sol–gel method, templated method and hydrothermal method, has greatly increased the prospects for the application of PLNPs in biomedical fields.

Sol–gel method

The "sol–gel method" refers to the hydrolysis of the precursor into a sol, which is then converted into a gel for subsequent calcination (800–1100 °C), resulting in high yields of small-sized and homogeneous PLNPs. In this process, generally speaking, in addition to the use of metal or alcohol salts as precursors, citric acid as a chelating ligand and alcohols as cross-linking agents are needed. At higher synthesis temperatures, small nanocrystals are squeezed into the discrete space provided by the complexing agent, limiting the growth of the nanocrystals and resulting in PLNPs [28].

Early in 2007, Shermont et al. developed the first sol–gel method to synthesize NIR PLNPs of $Ca_{0.2}$ $Zn_{0.9}$ $Mg_{0.9}$ Si_2O_6:Eu^{2+}, Dy^{3+}, Mn^{2+} with a size distribution of 50–100 nm for in vivo imaging [30]. They acidified the chloride and nitrate solutions with concentrated nitric acid, followed by the rapid addition of ethyl orthosilicate (TEOS) and stirring, which allowed the sol–gel transition to occur through heating, and ultimately, the particles were isolated by selective precipitation. At a pH of 2, the obtained particles have a broad excitation band in the ultraviolet (UV) region, a large emission spectrum with a maximum intensity of 690 nm, and an in vitro afterglow time of up to 24 h. Subsequently, improved synthesis methods, such as the sol–gel-microwave route, sol–gel-combustion processing and sol–gel-template technology, were developed to inhibit the growth of nanocrystalline grains [29].

Templated method

The template method is a commonly used and well-established method for synthesizing PLNPs. In this method, mesoporous silica nanoparticles (MSNs) or carbon nanorods are used as templates, which are combined

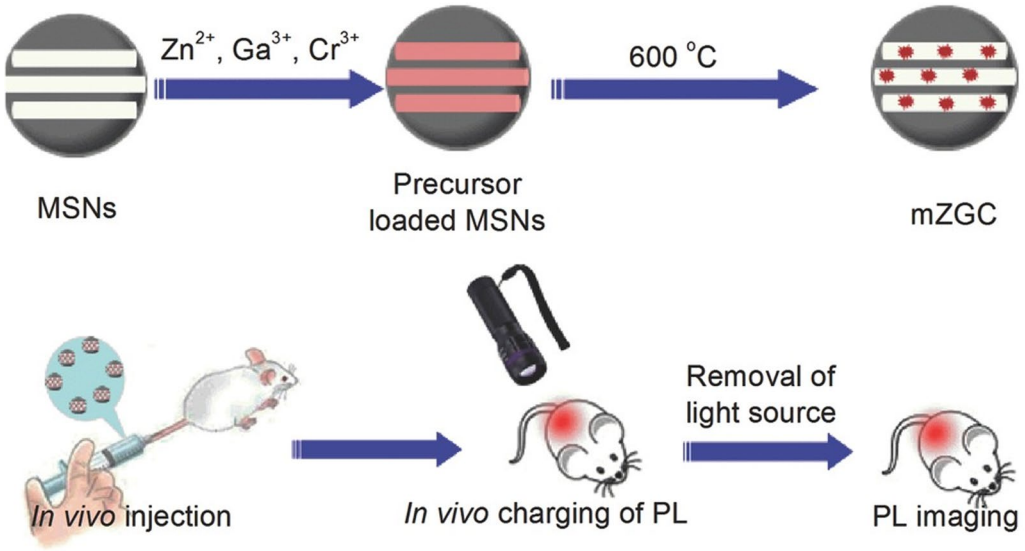

Fig. 1 Illustration of the synthesis of PL-functionalized MSNs and their in vivo imaging application. Reproduced under terms of the CC-BY license [31]. Copyright 2015, Wiley

with precursor ions and calcined at low temperatures, thereby obtaining PLNPs with controllable particle sizes, regular morphologies and monodispersities [31]. In addition, the presence of silica provides more possibilities for subsequent functionalization to modify PLNPs.

In 2015, Zhang et al. used MSNs as templates for the in situ synthesis of NIR PLNPs, SiO_2 / $ZnGa_2O_4$:Cr^{3+} (mZGC). After UV (254 nm) irradiation for 5 min, NIR fluorescence (696 nm) could still be detected after 5 h [31]. Because the conventional solid-state annealing temperature at 750 °C may lead to structural collapse of the MSNs, they reduced the reaction temperature to be 600 °C to maintain the nanostructure of the MSNs. A schematic of the synthesis process and in vivo deep tissue imaging of the synthesized PL-functionalized MSNs are shown in Fig. 1. In 2018, they subsequently used purgeable and highly dispersed carbon spheres as templates to synthesize NIR PLNPs of $ZnGa_2O_4$:$Cr^{3+}$with a large cavity, which can be loaded with doxorubicin (DOX) or photosensitizers to achieve an effective tumor suppression effect [32]. The synthesized hollow PLNPs are approximately 50 nm in size and produce intense NIR emission at 696 nm under 254 nm excitation, with an afterglow duration of more than 30 min.

More importantly, the high calcination temperature destroys the surface functional groups of PLNPs, which can lead to poor dispersion and undesirable stacking of PLNPs, thus limiting their application in biomedical fields to a certain extent [22].

Hydrothermal method

Unlike other synthesis methods, hydrothermal synthesis usually prepares PLNPs via chemical reactions in a dedicated high-pressure reactor, which provides a high-pressure and hermetically sealed environment throughout the reaction process, thus facilitating the reactions between the solid precursors [28]. The reaction time and temperature can be well controlled by this method, which allows the synthesis of highly crystalline PLNPs under relatively mild conditions. Importantly, the PLNPs synthesized via this method are ultrasmall in size and easy to surface modify. Successful synthesis via the hydrothermal method is influenced by several important factors, such as high processing temperatures, organic additives, surfactants, etc., with specific functional groups, including oleic acid, polyethylenimine (PEI), ethylenediaminetetraacetate (EDTA), and cetyltrimethylammonium bromide (CTAB).

Han et al. reported a direct hydrothermal method for the synthesis of NIR PLNPs at 220 °C in 2015 [33]. The synthesized $ZnGa_2O_4Cr_{0.004}$ PLNPs are less than 10 nm in diameter and can form stable colloidal solutions in aqueous solution with an in vivo afterglow duration of more than 30 min. In addition, the size of the synthesized PLNPs can be controlled by adjusting the Zn/Ga molar ratio in the solution. In 2017, Yuan et al. reported $Zn_{1+x}Ga_{2-2x}Ge_xO_4$:Cr via a hydrothermal method, and the size and afterglow duration of PLNPs could be adjusted by adjusting the amount of Ge [34]. Although hydrothermal methods have great advantages in terms of particle size, dispersion, and functionalization, they still

suffer from the drawbacks of weak afterglow intensity and short afterglow duration, which need to be improved upon by further research [28]. Finally, a comparison of the various synthesis methods in terms of luminescence intensity, afterglow duration, particle size, and morphology is given in Table 1.

The emerging synthesis methods

In addition to these previously introduced methods, researchers have successively proposed several novel synthesis methods to obtain smaller-sized and brighter PLNPs. A co-synthesis method was used by Richard et al. PLNPs precursors were synthesized via a hydrothermal method and subsequently calcined at 750 °C to prepare $ZnGa_2O_4$:Cr^{3+} with enhanced optical and physical properties [21]. In addition, the tuning of PLNP traps, size and water dispersibility by simple ethylenediaminetetraacetate (EDTA) etching was explored by Zhang et al. [35]. $Cr_{0.004}{}^{3+}$:$ZnGa_2O_4$ (ZGO) was used as a PLNP model, and EDTA etching of the sintered ZGO effectively reduced the size and greatly improved the degree of water dispersion. Besides, microwave-assisted heating has utilized for the synthesis of PLNPs, which greatly reduces the reaction time compared with the conventional heating in autoclave. The principle lies in the use of microwaves to heat the medium that can absorb waves in the reaction system to warm the reaction system. This synthesis method is not only simple and fast but also results in PLNPs with good physical properties. Pedroso et al. reduced the reaction time from 48 h to 30 min, which greatly improved the synthesis efficiency [36].

Organic PLNPs that do not rely on a limited number of rare earth elements are also a hot topic of current research. They are well known for their ability to be easily synthesized and modified, as well as their advantages of biocompatibility, long luminescence lifetime, and easy synthesis. However, organic PLNPs suffer from severe nonradiative leaps of excitons in the trilinear state and serious spin-forbidden blocking between the single and triplet excited states. Researchers usually inhibit the non-radiative leaps through crystal engineering, the introduction of rigid polymer matrices and cross-linking strategies; or promote intersystem crossing and increase spin–orbit coupling through the introduction of heavy atoms, heteroatoms and aromatic carbonyls [37].

Surface functionalization of PLNPs

Owing to limitations in synthesis methods and raw materials, PLNPs generally lack modifiable groups on their surfaces. The surface properties of nanomaterials have an important impact on their biomedical applications; thus, surface functionalization of PLNPs is essential to obtain better biocompatibility, lower cytotoxicity, stronger stability stabilization and facilitating further attachment of functional groups.

The use of silicon dioxide, especially MSNs coating is an important method for the surface functionalization of PLNPs. In addition to the template synthesis method described previously to obtain MSNs-coated PLNPs, Yan et al. added the synthesized $Zn_{1.2}Ga_{1.6}Ge_{0.2}O_4$:$Cr^{3+}$ (approximately 20 nm in diameter) together with sodium salicylate and CTAB into a triethanolamine solution and then stirred it with TEOS. Finally, silica-coated PLNPs were obtained after the addition of aminopropyltriethoxysilane [38]. Other methods of surface functionalization have also been reported. Fu et al. reported mesoporous polyacrylic acid (PAA)/calcium phosphate (CaP)-coated $Zn_{1.25}Ga_{1.5}Ge_{0.25}O_4$:0.5%Cr, 2.5%Yb, 0.25%Er for bioimaging of bacterial infections and chemotherapeutic treatments [39]. The passivation of the surface defects of the PLNPs by the PAA shell layer and the energy transfer between the shell layer and the PLNPs effectively prolonged the decay time of the PLNPs. As a result, the sustained luminescence intensity of the PLNPs was enhanced. In 2020, Chan et al. grafted polyaniline (PANI) and glycol chitosan (GCS) on the surface of synthesized PLNPs to synthesize PLNP@PANI-GCS, which is a pH switchable nanoplatform for in vivo persistent luminescence (PersL) imaging and precise PTT of bacterial infection. The pending positively charged nanoplatform

Table 1 Comparison of synthesis methods of PLNPs in terms of luminescence intensity, afterglow duration, particle size, and morphology

Synthesis methods	Luminous intensity	Afterglow duration	Particle size (nm)	Morphology	Refs
High temperature solid-state reaction	High	Long	Micron scale	Uneven size and irregular shape	[21, 28]
Sol–gel method	Medium	Medium	50–100	Uniform size, regular morphology,and controlled particle size	[28–30]
Templated method	Medium	Slightly shorter	50–500	Uniform size, regular morphology, monodispersity	[22, 31, 32]
Hydrothermal method	Weak	Slightly shorter	5–20	Uniform size, regular shape, good dispersion	[33, 34]

responds to acidic regions of bacterial infection and electrostatically binds to bacteria in vivo, ensuring spatial precision of NIR light irradiation. It has great potential for providing a targeted, nonautofluorescence imaging-guided, precisely visualized therapeutic approach for the treatment of multidrug-resistant bacterial infections [40]. In 2021, Li et al. used neutrophil delivery to penetrate the blood–brain barrier for ultrasound-enhanced chemotherapy/immunoglioblastoma treatment. $ZnGa_2O_4$:Cr^{3+} (ZGO) was coated with a hollow acoustic-sensitive TiO_2 shell with the ability to generate reactive oxygen species (ROS) and control drug release. Moreover, an immune checkpoint inhibitor of anti-PD-1 antibodies was loaded and further loaded into liposomes encapsulated with paclitaxel (PTX) [41].

Besides, the combination of multiple modification methods can also enable PLNPs to obtain more complex and flexible biological functions. For example, in 2023, Zhang et al. deposited ultrasound-excited mechanoluminescent nanodots of Sr Al_2O_4:Eu^{2+} (SAOE) and PersL nanodots of $ZnGa_2O_4$:Cr^{3+}(ZGC) on mesoporous silicate, followed by modification with NO donors loaded with polydopamine (PDA). Ultrasonication caused mechanoluminescence from SAOE to excite the ZGC PLNPs to emit NIR, which excited the PDA, generating a sustained autothermophoretic force to facilitate nanoparticle uptake. Moreover, NIR-stimulated PTT and PersL-triggered NO release achieve anti-tumor effects (Fig. 2) [42].

Optical properties of PLNPs

Persistent luminescence (PersL)

The most prominent optical property of PLNPs is PersL, which means that the material can quickly absorb the excitation energy and continue to emit luminescence for a certain period of time from minutes to hours and even days after the end of excitation [43]. The generation of PersL is now widely recognized to be associated with two important constituent elements and four processes. These include the generation of charge carriers, trapping of charge carriers, release of trapped charge carriers, and recombination of the released charge carriers to produce emission (Fig. 3) [44]. Emitters and traps play important roles in these four processes. Emitters usually consist of transition metal ions or lanthanide ions doped in a host material, which can form a ground state energy level and a series of excited state energy levels [45]. However, traps usually consist of intrinsic crystal defects and codopants that can trap and store charge carriers. Specifically, the mechanism of the PersL process is the energy transfer process of luminescence centers and trap centers formed by doping elements in the matrix during the preparation of PLNPs. When PLNPs are excited by an outside light source, the electrons in the luminescence centers absorb the energy generated by the excitation and transition to the excited state, and some of the electrons are captured by the trap centers. When the excitation stops, the electrons captured by the trap centers escape from the trap to the excited state and release energy to emit light [28]. Upon effective excitation (electron beams, X-rays, and UV light), the emitters absorb photons, are excited to a higher energy level and produce charge carriers such as electrons and holes [23, 46]. The charge carriers are then captured by traps in the crystal and can be stored for long periods. With thermal motion, optical stimulation, or other physical irritations, such as mechanical irritation, these captured charge carriers are slowly released from the trap to the ground state of the emitters, resulting in the phenomenon of PersL [47].

The factors affecting the PersL are closely related to two elements: the emitter and the trap. The luminescent properties of PLNPs are usually effectively controlled from these two aspects through electronic structure engineering [45]. The characteristics of the trap affect the duration and intensity of PersL [48]. Improving the trapping efficiency of traps, such as setting the right density of the trap distribution and choosing the right trap depth, can help to increase the number of trapped electrons and thus store more excitation energy, which makes it possible to realize longer-lasting, high-quality luminescence. For example, in 2021, Li et al. replaced Zn^{2+} with Li^+ in the Zn_2GeO_4 nanocrystals [49]. Li^+ easily occupies the Zn^{2+} positions in the crystals because of their similar ionic radius (76 pm for Li^+ and 74 pm for Zn^{2+}). The afterglow intensity changed depending on the Li^+ doping concentration and was positively correlated before the Li^+ concentration was increased to 30%. More original electron traps and a new type of electron trap with deeper depth were observed, both of which contributed to the enhancement of the PersL. In addition, we can add external defects through the introduction of different phenomena, such as the addition of a dopant. When $SrAl_2O_4$ is doped with Eu^{2+}, the afterglow is short-lasting and weak, but with the use of co-dopant Dy^{3+}, both the afterglow time and the intensity of emission increase [50]. The nature of the emitters also influences the PersL phenomenon. Emitters should be able to emit radiation effectively after absorbing energy. Therefore, enhancing the nature of the emitter can help extend the PersL time and increase the luminous intensity. Currently, two main methods are increasing the size of PLNPs and protecting them via shell coating [48]. In terms of increasing size, Jing et al. reported a hydrothermal synthetic route for preparing differently sized $ZnGa_2O_4$:Cr nanoparticles (NPs). According to

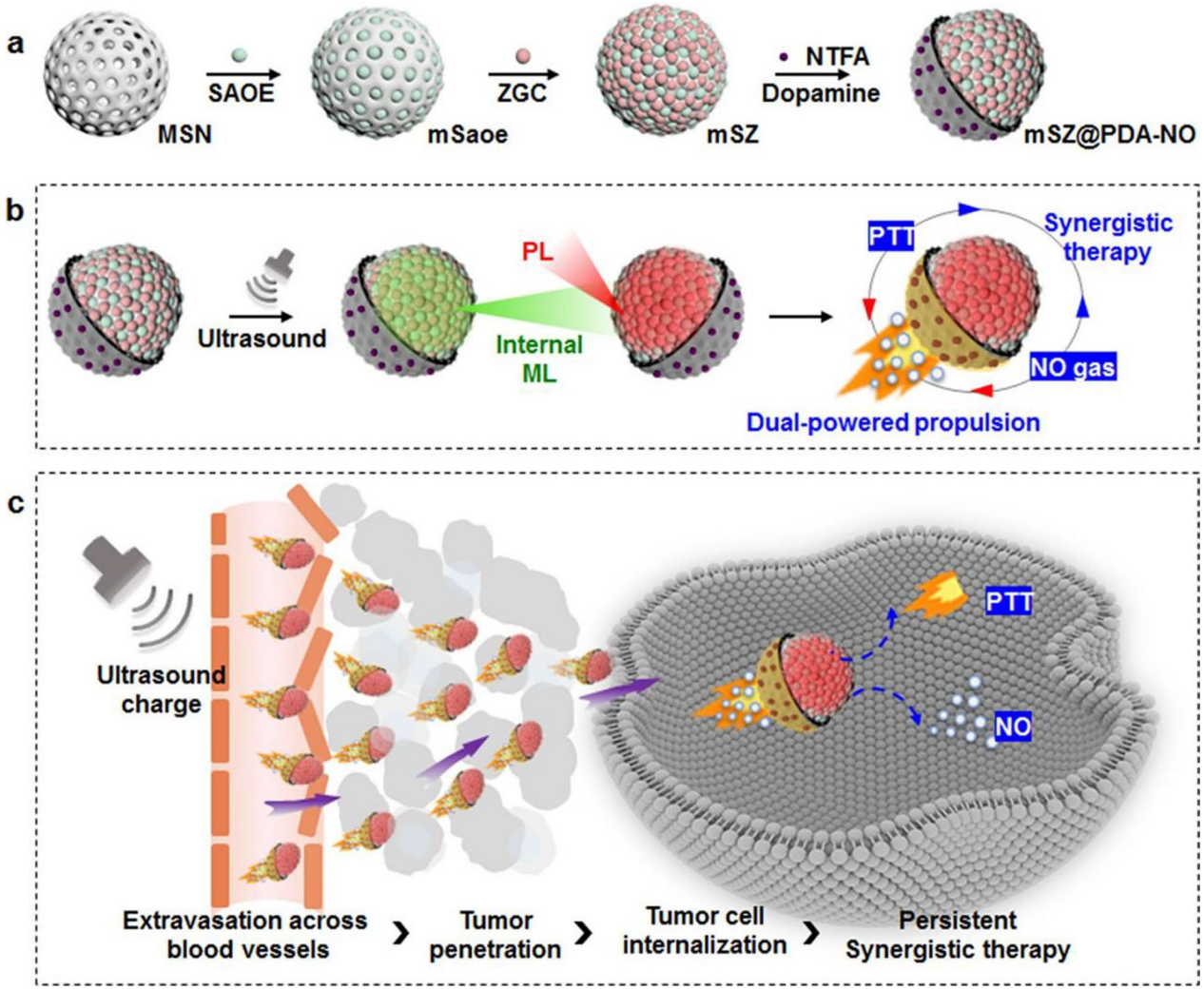

Fig. 2 Preparation and Treatment Mechanism: **a** SAOE nanodots deposited on MSNs, followed by ZGC nanodots to obtain mSZ NPs. PDA layers with NO donors selectively capped on one side of mSZ NPs to form Janus mSZ@PDA-NO NPs. **b** Ultrasonication of NPs generates ML green emission, which excite ZGC nanodots to emit NIR PL. **c** Internal NIR excitation of PDA caps produces persistent self-thermophoretic force to propel NP motion. Reproduced with permission [42]. Copyright 2023, American Chemical Society

the particle size-dependent luminescence and luminescence decay curves, dimensional changes can effectively increase the intensity of the PersL [51]. Similarly, increasing the size of $ZnGa_2O_4:Cr^{3+}$ (ZGO) or zinc gallogermanate (ZGGO) can also lead to an increase in the PersL response of PLNPs [52, 53]. For the method of shell coating, in 2021, Li et al. reported straightforward thermolysis-mediated colloidal synthesis of CaF_2:Dy@$NaYF_4$ core–shell PLNPs that can enhance PersL. Compared with the bare core CaF_2:Dy, the CaF_2:Dy core was well protected when the shell/core ratio increased to 0.5:1 and higher, accompanied by a 2–2.5 times increase in PersL efficacy [54].

Moreover, PLNPs can maintain luminescence after excitation even for days, a feature that allows imaging without in situ excitation [48]. Therefore, interferences from tissue autofluorescence are eliminated, which allows for an excellent signal-to-noise ratio (SNR) and significantly improved sensitivity, providing background-free signals for long-term bioimaging, such as cell tracing, highly sensitive in vivo imaging, and ultrasensitive detection [28, 55, 56].

Influence of excitation source on PersL

In the process of biomolecular detection and fluorescence imaging, when an external light source excites a fluorescent probe, the excitation light and the fluorescence

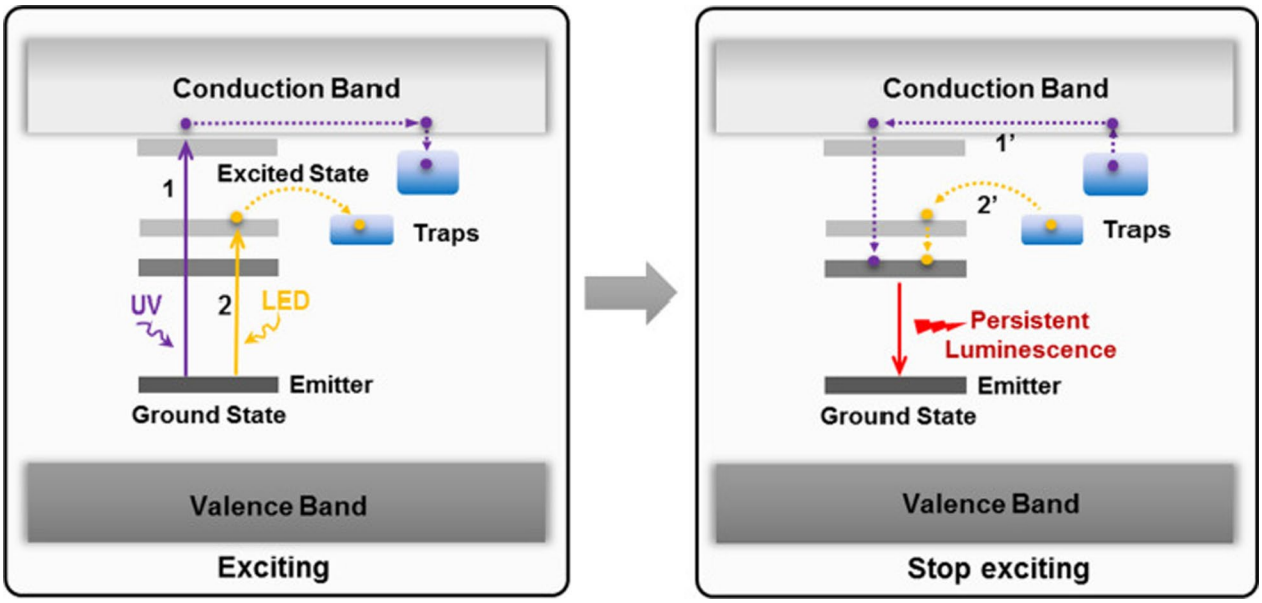

Fig. 3 Schematic diagrams of the PersL mechanism under different excitation sources. Reproduced under terms of the CC-BY license [28]. Copyright 2021, Springer Nature

emitted by the probe are partially scattered and absorbed by biological tissues. If the scattering and absorption increase, then accordingly, the depth of penetration of light into the tissues decreases, and the intensity of the fluorescent signal produced decreases. However, PLNPs can be excited by a variety of excitation sources, such as UV, light-emitting diodes (LEDs), NIR lasers, X-rays, and radiopharmaceuticals, which overcomes the problems of poor imaging quality and penetration depth caused by short-wavelength excitation (Table 2) [28].

Excitation sources are usually categorized into UV light, the visible region, the first NIR window (NIR-I, 700–900 nm), and the second NIR window (NIR-II, 1000–1700 nm) regions based on the wavelength [62]. Research has shown that the absorption coefficient of water increases in the NIR region, but at the same time, the scattering coefficient decreases for different types of tissues. Compared with those of visible light, the absorption coefficients of the main light-absorbing substances, such as water, hemoglobin, and lipids, are lower, which greatly increases the penetration depth of NIR light into tissues and avoids the problems of scattering generated by organisms [63]. Therefore, the wavelength range of the NIR region is called the "optically transparent window" of biological tissues, which refers to the wavelength range where the penetration depth of light in biological tissues reaches the maximum value, and it is the key region for obtaining high sensitivity, high resolution, and in vivo imaging effects. When the emission wavelength of the PLNPs is adjusted to the NIR region, the effects of low scattering and high detection depth are obtained.

However, even in the NIR region, penetration into tissues is limited, preventing in vivo excitation. Another approach is to use other excitation sources, such as X-rays. Compared with conventional excitation sources (UV/visible/NIR), X-rays offer the advantages of weaker scattering, deeper tissue penetration, and simplified image reconstruction from tomography. This allows us to achieve deeper tissue imaging and better spatial resolution [59].

Optical properties of novel PLNPs

With the further study of PersL and the rapid development of persistent phosphors, many now PLNP materials have been developed.

Metal–organic frameworks (MOFs) are emerging porous materials constructed via self-assembly of metal ions or clusters and multifunctional organic ligands. Owing to their tunable porosity structure, high specific surface area, low cost, various interaction sites, and well-designed functionalities, they have been widely used in molecular storage, catalysis, separation, optoelectronics, chemical/physical sensing, bioimaging, and oncology therapy [64]. In particular, it is favorable for the encapsulation of a wide range of molecules, including various drugs. When MOFs are combined with PLNPs, precise imaging and drug delivery can be achieved at the same time, which is promising for tumor therapy. For example, in 2019, Zhao et al. produced PLMOF (PLNPs@ZIF-8)

via in situ growth of MOF on PLNPs via a surface adsorption-induced self-assembly method. This combination enables PersL without external irradiation, providing deep tissue penetration and background-free interference imaging. Moreover, the remarkable drug-carrying capacity of the porous framework ZIF-8 results in drug release at the tumor site. It provides a good platform for precision tumor treatment [65]. In 2020, Yang et al. coated a PLNP surface with MOF UiO-66 to form a PLNP@UiO-66 core–shell composite, followed by calcination, and synthesized a macrophage membrane coated with PersL nanoparticle@MOF-derived mesoporous carbon core–shell nanocomposites (PLMCs) via the pyrolysis of UiO-66 shells. This compound shows great potential in drug encapsulation and luminescence imaging-guided chemotherapy [66]. In 2023, Zhao et al. reported a PersL MOF (PLNPs@MIL-100(Fe)) with a core–shell structure through a layer-by-layer method. Animal studies have shown that the PLNP core is capable of PersL without outside radiation, and the MIL-100(Fe) shell structure demonstrated high drug loading and controllable drug release capacity (Fig. 4) [67]. However, novel PLNP materials based on MOFs still face some challenges that need to be overcome. Controlling their shape and size is still challenging, but the size, morphology and structure of MOFs affect the luminescent properties of materials.

NIR PLNPs are emerging optical materials. They can emit NIR light for a long time after excitation and prevent autofluorescence. Furthermore, as mentioned above, the wavelength range of the NIR is within the "optically transparent window" of biological tissues, which allows for greater depth of tissue penetration, thus improving the sensitivity of biosensing and bioimaging. For example, in 2017, Zeng et al. proposed a new type of X-ray-activated $ZnGa_2O_4$:Cr PLNPs (X-PLNPs) which exhibited long-lasting up to 6 h NIR emission after excitation. Through the injection or oral administration of X-PLNPs after in situ activation, long-term deep-tissue in vivo bioimaging capabilities were demonstrated, which provided a new approach for overcoming the short decay time of PLNPs [57]. Cr^{3+}-doped $ZnGa_2O_4$ (ZGC) NPs are among the most representative NIR PLNPs. They have attracted widespread attention for their excellent PersL properties, high chemical stability, and variable excitation light sources [68]. In 2017, Huang et al. reported SiO_2@$ZnGa_2O4:Cr^{3+}$@SiO_2 PLNPs with high luminescence intensity and a long afterglow time through a silica template method. The PLNPs not only enhanced the NIR PersL properties but could also be repeatedly activated in situ by soft X-rays and continue to emit NIR for up to 12 days [69]. In 2020, Zhao et al. prepared PLNPs ($Zn_{1.1}Ga_{1.8}Ge_{0.1}O4:Eu_{0.009}$, $Cr_{0.09}$) via a hydrothermal method and combined them with alginate hydrogel to create PLNPs-containing hydrogels (PL-gel) for tumor-specific labeling and tracking of tumor metastases without autofluorescence. When combined with 4-carboxyphenylboronic acid, they can target MBA-MD-231 breast cancer cells, providing an effective way of revealing the tumor metastasis process [70]. Many current NIR PLNPs are limited to single-wavelength emission, and the PersL of PLNPs can be applied only to bioimaging or PDT; most of the time, the two cannot be effectively realized at the same time. Therefore, the design of nanoplatforms with multifunctionality for both bioimaging and PDT is important for

Table 2 Comparison of the comparison of the penetration depth of different excitation sources

Year	PLNPs	Excitation	Penetration depth	Emission wavelength (nm)	PersL duration	Application	References
2015	$ZnGa_2O_4Cr_{0.004}$	White LED	10 mm pork	696 nm	15 min	NIR PersL bioimaging in vivo	[33]
2017	$ZnGa_2O_4$: 1%Cr	X-ray	20 mm pork	700 nm	6 h	PersL bioimaging in vivo	[57]
		White LEDs	6 mm pork	700 nm	10 h		
		365 nm UV laser	3 mm pork	700 nm	7 h		
2017	PEG-$SrAl_2O_4$: Eu^{2+}	X-ray	25 mm pork	530 nm	2 h	Bioimaging of deep-tissue in vivo	[58]
2018	ZGO:Cr/W PLNPs	X-ray	20 mm pork	693 nm	6 h	PDT in vitro and in vivo	[59]
2017	$Zn_{1.1}Ga_{1.8}Ge_{0.1}O_4$: 0.5%Cr	980 nm NIR laser	10 mm pork	700 nm	5 min	Lymphatic PersL Imaging in Vivo	[60]
		254 nm UV laser	< 5 mm pork	700 nm	5 min		
		365 nm UV laser	< 5 mm pork	700 nm	5 min		
		White LED	< 5 mm pork	700 nm	5 min		
2023	$Zn_{1-x}(Li/Ga)_xGa_2O_4$: $0.005Cr^{3+}$	740 nm NIR laser	20 mm pork	718 nm	25 min	PersL bioimaging in vivo	[61]

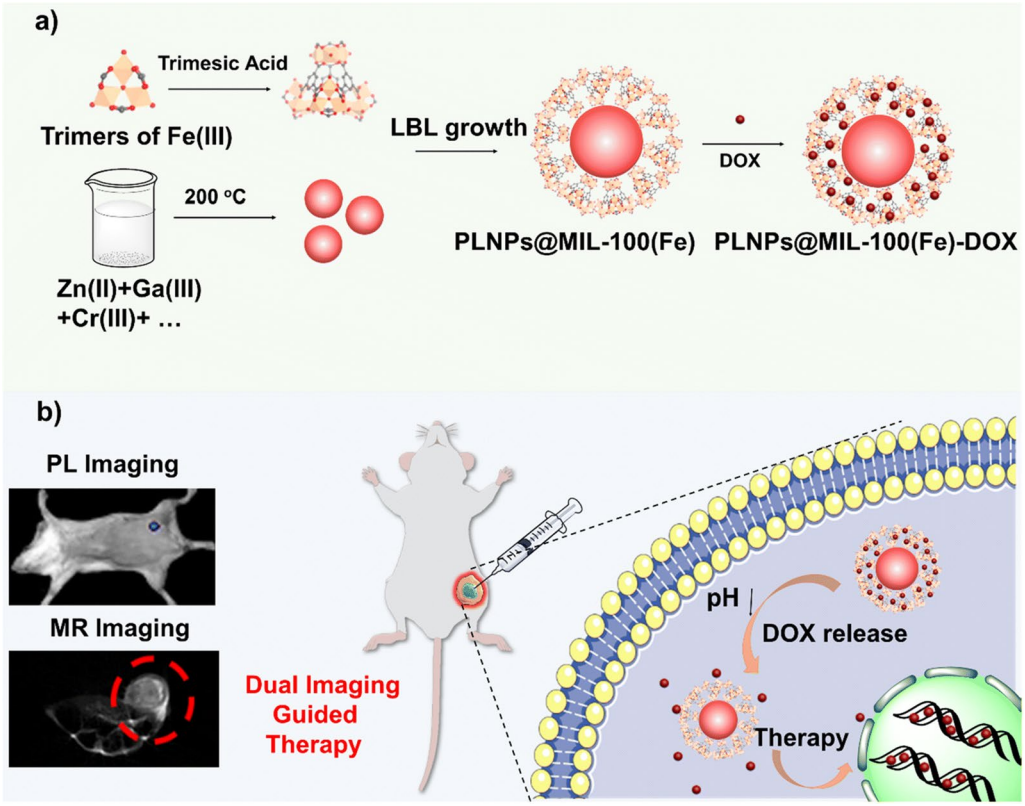

Fig. 4 Schematic illustration for the preparation of PLNPs@MIL-100(Fe) NPs for PersL/magnetic resonance (MR) dual-modal imaging and drug delivery. Reproduced with permission [67]. Copyright 2023, Royal Society of Chemistry

the precision treatment of tumors. In 2022, Sun et al. proposed X-ray-excited PLNPs ($Zn_3Ga_2Ge_2O10:Cr^{3+}$, Mn^{2+}, ZGGCM) with dual functions for in vivo PersL imaging and PDT. These results indicated that Cr^{3+} ions in ZGGCM provided good NIR PersL imaging performance, whereas the green PersL emission peak of Mn^{2+} ions effectively promoted the generation of ROS to achieve significant antitumor effects. This nanomaterial facilitates the development of an integrated tumor diagnostic and therapeutic approach [71]. In 2024, Abdukayum et al. combined PLNPs ($LiGa_{4.99}O_8:Cr_{0.01}$, LGO: Cr) with iridium oxide NPs (IrO_2 NPs) covalently to produce multifunctional nanoplatforms with simultaneous NIR PersL, PDT and PTT effects (Fig. 5) [72].

Biocompatibility of PLNPs

At present, PLNPs for biomedical applications are biocompatible because of their prolonged retention in normal tissue. Thus, a good understanding of the pharmacokinetics and biosafety of PLNPs in biological systems can greatly promote the biomedical applications of PLNPs for future clinical translation. To date, multiple cell lines have been used to evaluate the in vitro cytotoxicity of different PLNPs. Most of the results indicated that the PLNPs had no obvious cytotoxicity. Jing-Min Liu et al. incubated three cell types, Balb/3T3, HeLa and MCF-7, with PLNPs at concentrations ranging from 50 to 1000 $\mu g \cdot mL^{-1}$ for 24 h. The viability was determined to be greater than 85% after incubation, confirming the relatively low toxicity of the PLNP nanocarriers [73].

Biomembrane-modified PLNPs can effectively enhance the biocompatibility of PLNPs [22]. Li et al. studied the in vitro cytotoxicity of CCM-coated PLNPs, and the PDT-controlled cytotoxicity of DSPLNPs@$hSiO_2$@CCM was evaluated in 4T1 cells. CCM, SPLNPs@$hSiO_2$, and SPLNPs@hSiO2@CCM up to 50 $\mu g \cdot mL^{-1}$ showed negligible cytotoxicity and did not cause pathological changes in organs [74].

In 2021, Wang et al. synthesized ultrasmall PLNPs with an average diameter of 2.5 nm using MSNs as the template [75]. After further coating with polyethylene glycol (PEG), the diameter of the PLNPs-PEG increased to 5.0 nm and exhibited excellent PersL performance under 254 nm UV light irradiation. After injection into live nude mice via the tail vein, PLNPs-PEG was effectively metabolized by the kidneys within 24 h and did not cause damage or inflammatory changes in the main

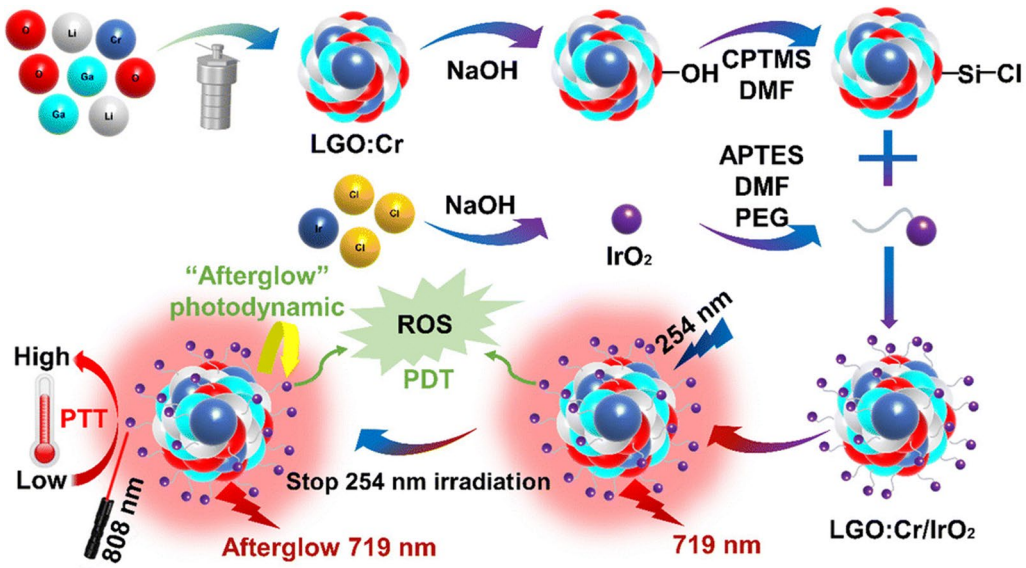

Fig. 5 Schematic construction of a multifunctional nanoplatform of LGO:Cr/IrO2 with NIR sustained luminescence, and "afterglow" PDT and PTT capabilities. Reproduced with permission [72]. Copyright 2024, Royal Society of Chemistry

organs (heart, liver, spleen, lung, kidney, or intestines) of the mice after 14 days.

The possible mechanisms of tissue damage caused by NPs include cell morphology and cytoskeleton changes, oxidative stress, genotoxicity, and tissue damage caused by the illumination requirements of NPs application [76, 77]. Tissue damage caused by long-term in situ excitation light sources can be avoided because of the long-term luminescence of PLNPs after excitation. The mechanism of oxidative stress involves the recognition and response of NPs as foreign substances by immune system cells, resulting in the production of ROS, and high concentrations of ROS for a long period of time mediate damage to or death of various types of cells [78, 79]. There are lots of studies on the effect of PLNPs on biological safety via ROS-related mechanisms, and ROS levels can be assessed via the use of fluorescent probes such as dihydrofluorescein and its derivatives. The process of NPs uptake by cells and the occupation of the intracellular volume may cause changes in cell morphology and the cytoskeletal network [80]. Gene level changes are based on mechanisms such as high levels of ROS or induced cellular stress induced by NPs [81]. There are relatively few studies on the genotoxicity and morphological effects of PLNPs, and further research is needed.

In order to reduce tissue damage, surface modification is used to increase the biocompatibility of PLNPs. In 2017, Ramírez-García et al. evaluated the acute (24 h), short-term (30 days) and long-term (6 months) toxicological effects of PLNPs in vivo in terms of oxidative stress, cell and tissue morphology, and DNA levels, aiming to verify the effects of surface modification on the biocompatibility of PLNPs [82]. They modified $ZnGa_{1.995}Cr_{0.005}O_4$ by hydroxylation and PEGylation to obtain ZGO-OH and ZGO-PEG, respectively. They were injected into BALB/c mice via the tail vein. An extremely high concentration of 8 mg/mouse caused weight loss, a significant increase in white blood cells, and liver tissue damage caused by oxidative stress in the mice. All other concentrations did not result in abnormal parameters throughout the 6 months. These results demonstrated the protective effect of PEG functionalization of PLNPs and the safety of the application of PLNPs in vivo.

Application of PLNPs in tumor imaging

Tumor imaging of PLNPs based on cellular and biomolecular levels

PLNPs exhibit excellent optical properties, high sensitivity and good biocompatibility, thus offering unique advantages in the selective imaging of tumor cells in vitro. To target tumor cells, various ligands, such as biotin (BT), folic acid (FA), antibodies, aptamers and peptides, have been anchored on the surface of PLNPs [83–86]. In 2020, Yang et al. prepared NIR-emitting PLNPs ($Zn_{1.1}Ga_{1.8}G_{e0.1}O_4$:$Eu_{0.009}$, $Cr_{0.09}$) through a hydrothermal method and then modified them with 4-carboxyl phenylboronic acid, which is specific to the sialic acid receptor of MDA-MB-231 metastatic breast cancer cells. Compared with smooth muscle cells and macrophages, tumor cells exhibit significantly stronger luminescence [70]. In 2021, aptamer-containing DNA was conjugated with Au-coated PLNPs to target the overexpressed

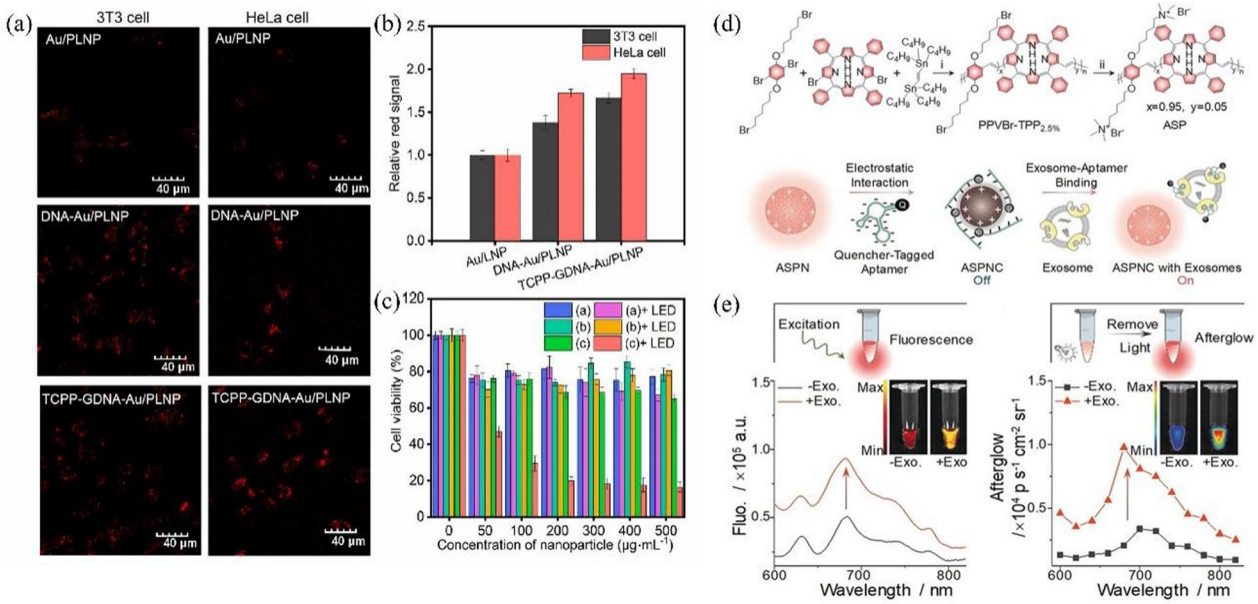

Fig. 6 **a** Confocal laser scanning microscope (CLSM) images of the HeLa and 3T3 cells treated with Au/PLNP, DNA-Au/PLNP and tetrakis (4-carboxyphenyl) porphyrin (TCPP) and G-quadruplex structure (GDNA) -Au/PLNP (TCPP-GDNA-Au/PLNP). **b** Relative luminescence intensity of the HeLa and 3T3 cells treated with Au/PLNP, DNA-Au/PLNP and TCPP-GDNA-Au/PLNP (The detailed red signal intensity was calculated by Image J software with the same amount of cells and the luminescence intensity of the cells treated with Au/PLNP was taken as 1). **c** Cell viability of the HeLa treated with Au/PLNP (a), DNA-Au/PLNP (b) and TCPP-GDNA-Au/PLNP (c) with or without 650 nm LED irradiation. (D) CLSM images of HeLa cells incubated with Au/PLNP, DNA-Au/PLNP and TCPP-GDNA-Au/PLNP with or without 650 nm LED irradiation. Reproduced with permission [87]. Copyright 2021, Elsevier. **d** Illustration of sensing exosomes using afterglow signal of the nanocomplex (ASPNC). **e** Fluorescence and afterglow spectra of ASPNC with and without exosomes. Reproduced with permission [90]. Copyright 2019, Wiley

nucleolin of HeLa cells (Fig. 6a-c) [87]. In 2022, Song et al. synthesized zinc-doped silica nanospheres (Zn@SiNSs) with ultralong phosphorescence via a hydrothermal method. RGD (Arg-Gly-Asp) peptides were functionalized on Zn@SiNSs, which could target highly expressed integrins of human glioblastoma cells and achieve a high signal-to-background ratio (≈69) imaging [88]. Introducing dual-targeting ligands to PLNPs is attractive for improving their specificity toward tumor cells. For example, $ZnGa_2O_4$:Cr,B PLNPs synthesized via a hydrothermal method were modified with hyaluronic acid (HA) and FA to provide synergistic targeting effects, which led to brighter luminescence signals than single- or nontargeting ligand-functionalized PLNPs in the NIR region after the imaging of MCF-7 breast cancer cells [89].

PLNPs can also serve as nanoprobes for imaging signal molecules in tumor cells. H_2S has been proven to be an important endogenous signaling molecule that plays a role in tumor development. In 2020, Suzuki et al. reported NIR organic PLNPs for imaging H_2S in hepatic cancer cells (HCCs). They employed EM $F1^{2+}$ as a H_2S-responsive chromophore and integrated it with the photosensitizers NIR775 and poly[2-methoxy-5-(2-ethylhexyloxy)-1,4-phenylenevinylene]. After specific ligands are introduced on the surface, this probe can efficiently enter HCCs, and the afterglow intensity increases with increasing intracellular H_2S levels [91]. Epidermal growth factor receptor (EGFR) activation is related to various tumor biological processes, such as tumor cell proliferation, angiogenesis and metastasis. In 2022, Sun et al. developed a PLNP-based probe to observe EGFR-related signaling pathways in lung cancer cells. The electron transfer from the ligand of EGFR to $ZnGa_2O_4$ PLNPs mediated by the ferrocene-DNA polymer chain could trigger afterglow signals, and this probe allowed dynamic monitoring of the EGFR signaling pathway during tumor cell division [92].

Many sensors based on PLNPs have also been developed for in vitro detection of tumor markers because they show great advantages in eliminating the background fluorescence noise of complex samples. These biosensors often involve fluorescence resonance energy transfer (FRET) from PLNPs to the receptor. Quenchers are commonly used as receptors to quench luminescence. When tumor markers are present as competitors, the FRET system is destroyed, and the luminescence signal is restored. For example, in 2020, Zhao et al. doped Mn^{2+} in Zn_2GeO_4 to prepare green-emitted ZGO:Mn PLNPs and doped Cr^{3+} in $ZnGa_2O_4$ to prepare NIR-emitted

ZGC PLNPs. Aptamers of prostate-specific antigen (PSA) and carcinoembryonic antigen (CEA) were subsequently functionalized on the surfaces of the ZGO:Mn and ZGC PLNPs, respectively. The luminescence signals of the two PLNPs were quenched by PDA NPs and recovered in the presence of PSA and CEA, which provided a new method for high-throughput tumor marker detection in serum samples [93]. In another study, Yuan et al. presented a PLNPs-based biochip for the sensitive detection of bladder cancer-related miRNA-21 (miR-21). The ZGO:Mn PLNPs were conjugated with single-stranded DNAs (cDNAs) complementary to miR-21 and further hybridized with black-hole-quencher-labeled (BHQ) DNAs (BHQ-DNAs). When samples containing miR-21 were added, BHQ-DNAs were separated from the PLNPs because of the specific binding between the cDNAs and miR-21, thus turning on the afterglow signals. In addition, this luminescence probe was linked to the photonic crystal substrate to amplify luminescence signals, which could achieve a detection limit of 26.3 fM in human urine [94]. Interestingly, Pu et al. also applied PLNPs for the detection of tumor exosomes. They synthesized a poly(p-phenylene viny-lene)-based NIR afterglow semiconducting polyelectrolyte was passed and employed a BHQ-tagged aptamer as the quencher. Similarly, exosomes could trigger the recovery of luminescence signals, and the limit of detection was nearly two orders of magnitude lower than that of common fluorescence detection (Fig. 6d–e). This sensor was able to distinguish exosomes from different cells and could be used for the identification of tumor cells [90]. In addition to the above quenchers, fluorescent molecules can also be used as receptors for PLNPs. In 2015, Yan's group used a PSA antibody (PS6)-modified PLNP as the energy donor and another PSA antibody (8A6)-modified rhodamine B (RhB) as the acceptor to construct a fluorescent probe. The specific binding of PSA with antibodies mediated FRET from PLNP-PS6 to RhB-8A6 and enabled the PLNPs to excite RhB, thus realizing sensitive ratiometric photoluminescent detection of PSA in serum and cell extracts [95].

Tumor imaging of PLNPs in vivo

Direct modification of relevant targeting molecules on PLNPs can result in direct targeting of tumor cells, and the NPs used for tumor labeling must possess specific characteristics and be considered for practical application in vivo. The appropriate dimensions and morphology significantly affect their distribution and uptake within the tumor tissue. Surface modification is crucial to ensure targeting ability in the tumor microenvironment. Optical properties are also important for high-resolution imaging and precise localization within tumor tissue. Biocompatibility is essential for toxicity or immune reactions. The targeting capability can be achieved through the incorporation of molecules that specifically bind to imaging specificity. Moreover, achieving efficient conversion of light into heat while maintaining thermal stability is necessary. Finally, it is crucial for NPs to exhibit favorable solubility and stability under physiological conditions to ensure prolonged circulation time and accurate imaging capabilities within the tumor tissue [96].

PLNPs are capable of absorbing and retaining excitation energy, subsequently releasing it as PersL, which persists for an extended duration following cessation of excitation. They allow in vivo imaging without autofluorescence, with a high target-to-background ratio and no need for in situ excitation. Thus, it has significant advantages in in vivo tumor imaging. In 2024, Liu et al. unveiled a multifunctional nanoplatform based on $LiGa_{4.99}O_8{:}Cr_{0.01}/IrO_2$, which exhibits diverse functionalities, including NIR PersL, photodynamics, and PTT. This platform is formed through covalent bonding between a persistent luminescent nanoparticle $LiGa_{4.99}O_8{:}Cr_{0.01}$ and an iridium oxide nanoparticle IrO_2, enabling the generation of a laser-induced photothermal effect at 808 nm as well as sustained photodynamic effects without in situ excitation due to persistent energy transfer (Fig. 7) [72].

For the majority of NPs, in the absence of a specific surface coating, they undergo rapid opsonization and are subsequently captured by the liver following systemic administration in small animal models. In 2020, Liu et al. focused on the coating of PLNPs with hydrophilic polymers for in vivo imaging. A highly hydrophilic polymer of poly(N-2-hydroxypropyl) methacrylamide (pHPMA) has the ability to delay capture by the liver and prolong circulation in the bloodstream. Finally, preliminary in vivo imaging was performed in healthy mice injected with PLNPs encapsulated with pHPMA, where luminescent signals could be detected throughout the animal for up to 60 min, demonstrating the ability of the material to circulate in the bloodstream (Fig. 8) [97]. The excitation bands of previous PLNPs were typically located during UV region, leading to significant tissue damage and limited tissue permeability [45]. As mentioned above, NIR PLNPs have shown low scattering and absorption coefficients in penetrating biological organs or tissues and do not require continuous excitation light irradiation, which can effectively reduce the damage caused by light irradiation to tissues. Additionally, the reactivation of PersL in NIR PLNPs can be achieved via red or NIR light. This characteristic enables the utilization of NIR-emitting PLNPs for long-term bioimaging without being constrained by the limited lifetime of PersL [32, 98]. In 2013, Abdukayum et al. prepared $Zn_{2.94}Ga_{1.96}Ge_2O_{10}{:}Cr^{3+}$, Pr^{3+} PLNPs with NIR luminescence through co-doping of Pr^{3+}

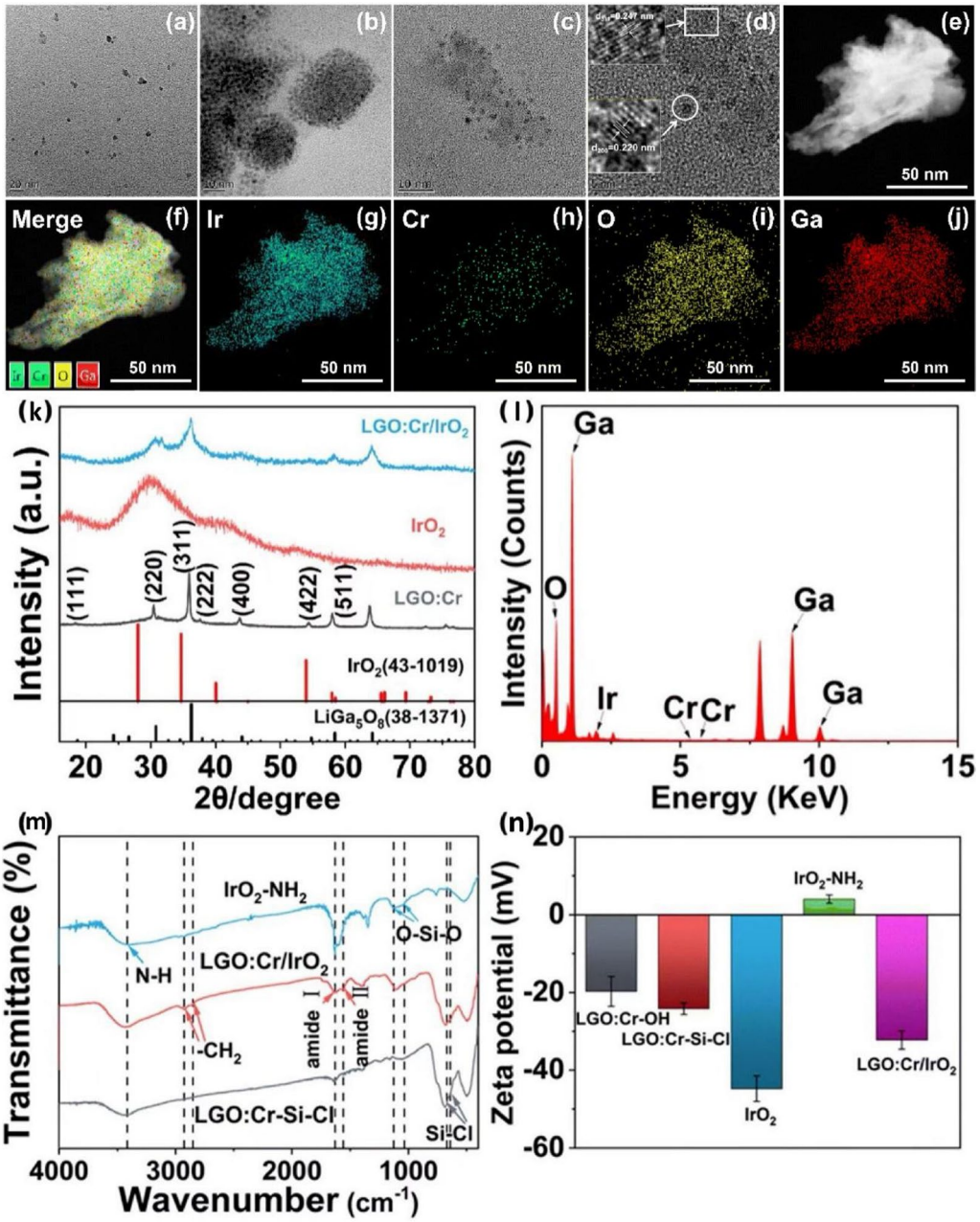

Fig. 7 Transmission Electron Microscope images of the **a** LGO:Cr, **b** IrO_2 NPs, and **c** LGO:Cr/IrO_2 composites. **d** High Resolution Transmission Electron Microscope images of LGO:Cr/IrO_2. **e**–**j** energy dispersive spectroscopy (EDS) elemental mapping of LGO:Cr/IrO_2. X-Ray Diffraction patterns of **k** LGO:Cr, IrO_2 NPs, and LGO:Cr/IrO_2 composites; and **l** EDS analysis of LGO:Cr/IrO_2. **m** Fourier Transform Infrared Spectroscopy spectra of LGO:Cr–Si–Cl, IrO –NH, and LGO:Cr/IrO. **n** Zeta potentials of LGO:Cr and IrO NPs with different surface modifications. Reproduced with permission [72]. Copyright 2024, Royal Society of Chemistry

and Cr^{3+}. Additionally, they improved the biocompatibility and water solubility of PLNPs through the incorporation of modified PEG. These PLNPs demonstrate an exceptionally prolonged afterglow duration, making them highly promising for extended in vivo targeted tumor imaging when combined with peptides. By chemically linking the RGD peptide of c through covalent conjugation, the increased binding affinity of PLNPs leads to an extended period of targeted tumor imaging in vivo [55]. HA receptors are commonly overexpressed on the surface of certain cancer cells. Similarly, FA receptors are similarly overexpressed in various types of cancers [99,

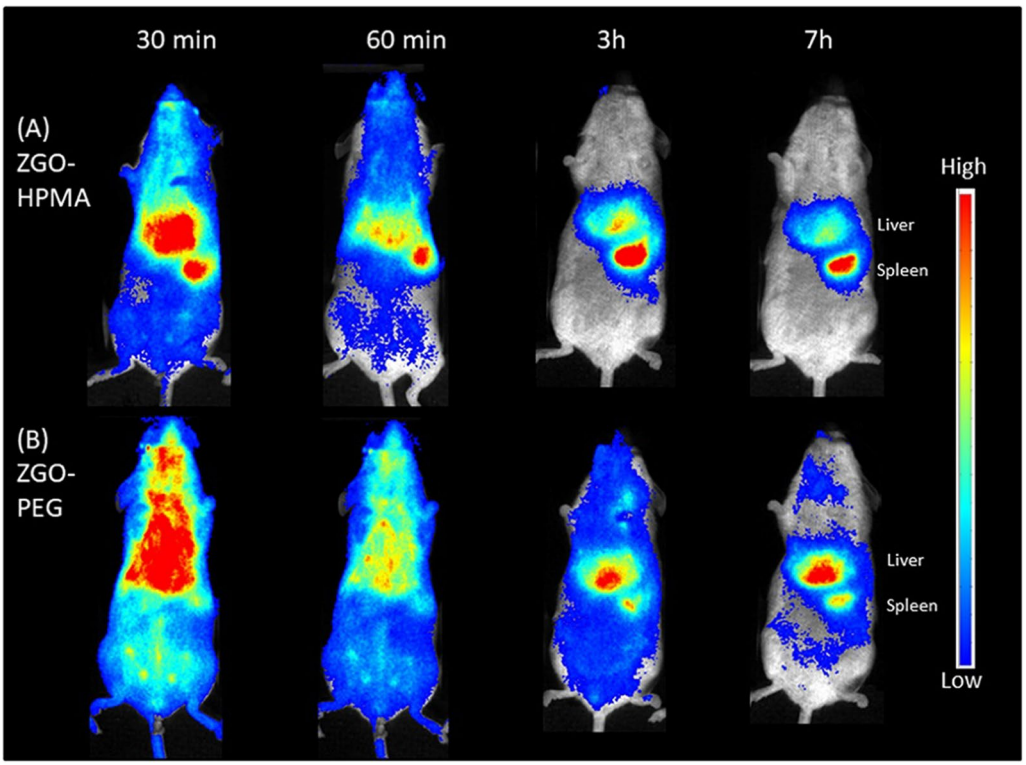

Fig. 8 In vivo biodistribution of coated ZGO in healthy mice. Reproduced under terms of the CC-BY license [97]. Copyright 2020, Frontiers Media S.A

100]. In 2016, Zhao et al. modified $ZnGa_2O_4$ NPs with chromium (Cr^{3+}) and boron (B^{3+}) ions and leveraged the specific binding affinities of ligands to target both HA and FA receptors on tumor cell surfaces. The combination of a dual-targeting strategy with the prolonged luminescence properties provided by the Cr^{3+} and B^{3+} co-doping system achieved high-resolution imaging of tumor cells with enhanced specificity and reduced false positives. The NPs exhibited excellent biocompatibility, and their hydrophilic surface modification improved the circulation time, thereby increasing their uptake in the target tumor tissue [22].

Finally, Table 3 the applications of the share of PLNPs mentioned above for re-tumor imaging, including their materials, absorption wavelengths, emission wavelengths, and imaging applications.

Application of PLNPs in cancer treatment

Photodynamic therapy based on PLNPs

At present, the applications of PLNPs in tumor therapy mainly include PDT, PTT, fluorescence-guided surgery and targeted drug delivery [22, 101]. Among them, PDT refers to the use of photosensitizers to generate ROS under specific wavelengths of irradiation, thereby killing tumor cells without damaging normal cells [102]. Currently, commonly used photosensitizers for PDT include porphyrins, chlorins, and phthalocyanines [103]. However, the application of traditional photosensitizers requires long-term light activation, which may lead to cell damage due to overheating [104]. Therefore, PLNPs with continuous luminescence after light excitation can reduce the applied dose of laser and minimize the adverse effects of light irradiation, which makes PLNPs ideal for application in PDT [23]. In addition, PLNPs show ideal biocompatibility, as mentioned above, which means that PLNPs do not significantly affect the viability of normal cells or tumor cells in the absence of light excitation. Under laser irradiation, PLNPs exhibit ideal antitumor properties. In addition, some PLNPs exhibit NIR optical properties. In biological imaging and PDT applications, NIR light nanomaterials have obvious advantages, as described above [105]. In 2016, Abdurahman et al. prepared Cr^{3+}-doped ZGGO (ZGGO:Cr^{3+}) as a NIR-excited PLNPs via a hydrothermal method and combined it with the photosensitizer silicon phthalocyanine (Si-Pc) (Fig. 9) [106]. Si-Pc-PLNPs showed the ability to continuously generate ROS at an excitation wavelength of 808 nm, resulting in a killing effect on HepG2 cells at 200 $\mu g \cdot ml^{-1}$. In 2017, Fan et al. prepared ZGC-PLNPs via a one-pot hydrothermal method and then combined

Table 3 A summary of published works about PLNPs-based tumor imaging

PLNPs	Surface coating	Excitationwavelength (nm)	Emission wavelength (nm)	Imaging application	References
$Zn_{1.1}Ga_{1.8}G_{e0.1}O_4$:$Eu_{0.009,}$ $Cr_{0.09}$	4-carboxyl phenylboronic acid	410	698	MDA-MB-231 metastatic breast cancer cells	[70]
$Zn_{1.25}Ga_{1.5}Ge_{0.25}O_4$:0.5%$Cr^{3+}$,2.5%$Yb^{3+}$,0.25%$Er^{3+}$	Aptamer-containing DNA, Au	Approx.420	694	HeLa cells	[87]
$ZnGa_2O_4$:Cr,B	HA,FA	254	650	MCF-7 breast cancer cells	[89]
Zn_2GeO_4:Mn	cDNA, BHQ-DNAs	269	535	Bladder cancer-related miRNA	[94]
Poly(phenylenevinylene)-based SPNs	Tetraphenylporphyrin (TPP), BHQ	520	680	Cancer exosomes	[90]
$LiGa_{4.99}O_8$:$Cr_{0.01}$	IrO_2	254	719	Vivo imaging	[72]
$ZnGa_2O_4$:Cr	Poly(N-2-hydroxypropyl) methacrylamide (pHPMA)	In UV or visible light range	679	Delaying the capture by the liver and prolonging the circulation in the blood-stream	[97]
$Zn_{2.94}Ga_{1.96}Ge_2O_{10}$:$Cr^{3+}$,$Pr^{3+}$	RGD peptide, PEG	254	695	An extended period of targeted tumor imaging in vivo	[55]

them with poly(lactic-co-glycolic acid)/N-methylpyrrolidone oleosol to obtain injectable PersL implants, which further improved the PersL intensity and lifetime [107]. In subsequent in vivo, the PersL implants changed from liquid to solid, which prolonged the retention time of the material in the tumor area of U87MG tumor-bearing mice. In addition, the PersL implants not only showed better imaging effects in vivo than ZGC but also produced ROS under LED irradiation. In 2018, Wang et al. prepared NIR PLNPs with hollow structures using a carbon sphere template as a template to carry the chemical drug DOX and the photosensitizer Si-Pc, which showed good in vitro and in vivo tumor killing effects via the production of singlet oxygen in PDT and the release of DOX [32].

Photothermal therapy based on PLNPs

Like PDT, PTT is also a common antitumor method that uses photoabsorbers to convert laser energy into heat under light irradiation for tumor cell killing (Table 4) [28]. In addition, the application of NIR in PTT has the advantages of strong tissue penetration and harmlessness. In 2017, Chen et al. combined NIR PLNPs of $ZnGa_2O_4$:Cr^{3+} (ZGC) and indocyanine green (ICG) into MSNs (Fig. 10) [108]. Among them, ZGC emits NIR light under UV light excitation for in vivo imaging. Moreover, the NIR light was absorbed by ICG and converted into heat, indicating an ideal antitumor effect of PTT in vivo. In 2021, Liu et al. used a hydrothermal method to prepare $ZnGa_2O_4$:Cr PLNP with two dual emission peaks at 508 nm and 714 nm for 1 h [109]. In addition, the authors used the strong adhesion of PDA and the electrostatic adsorption of 2,3-dimethylmaleic anhydride (DMMA) to functionalize PEG for the grafting of DOX. Under 808 nm laser irradiation, PLNP@PDA@DMMA/DOX showed strong tumor-killing effects both in vivo and in vitro, exerting dual anti-tumor effects of chemotherapy and PTT. In addition, the construction of dual-tumor effects of PDT and PTT based on PLNPs has also attracted widespread attention. In 2021, Zhao et al. prepared $Zn_{1.25}Ga_{1.5}Ge_{0.25}O_4$:0.5%$Cr^{3+}$, 2.5%$Yb^{3+}$, and 0.25%$Er^{3+}$ PLNPs via a hydrothermal method combined with the pH-reversibly responsive photosensitizer brominated asymmetric cyanine (BAC) and BT-functionalized PEG to prepare a multifunctional nanoplatform [110]. Under conditions of pH 6.0 and 808 nm laser irradiation for 10 min, obvious temperature changes and significant $^1O_2$ generation contributed to the effective in vitro and in vivo killing of human lung adenocarcinoma A549 cells and human cervical cancer HeLa cells.

Fluorescence-guided surgery based on PLNPs

With the increasing demand for tumor diagnosis and treatment, in order to achieve high treatment efficiency and few side effects, a biomedical system that integrates biological imaging and treatment into a single nanoplatform has been constructed for imaging-guided treatment. Bioimaging probes are among the most important parts of a treatment system and are responsible for identifying the location of tumor tissue, monitoring the biological distribution of nanoplatforms, and evaluating treatment effectiveness. Therefore, fluorescence-guided surgery (FGS), a surgical procedure guided by real-time

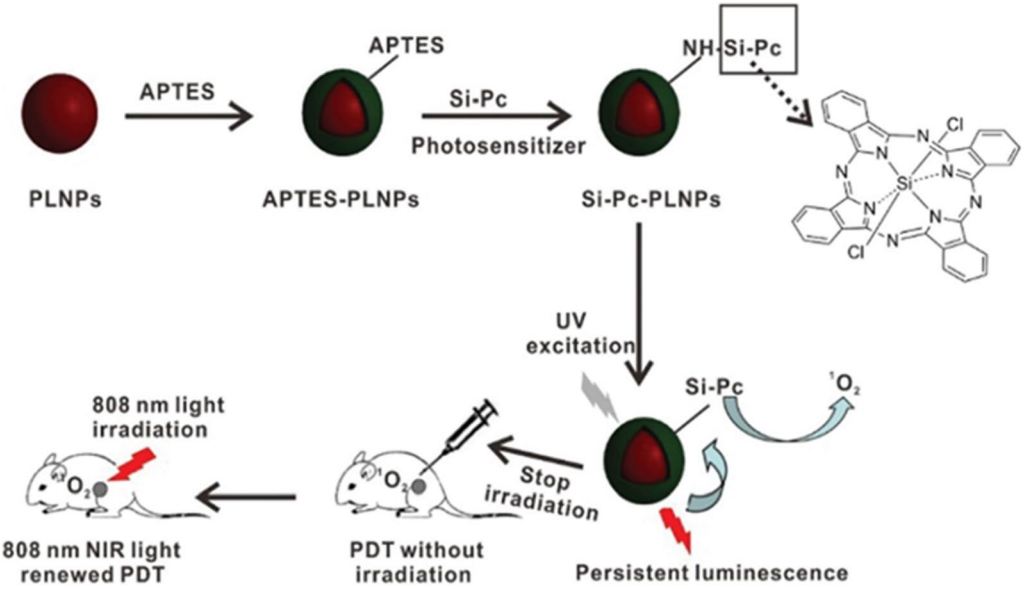

Fig. 9 Schematic illustration for the design of the 808 nm NIR light renewable PersL sensitized PDT platform. Reproduced with permission [106]. Copyright 2016, Royal Society of Chemistry

fluorescence images of diseases, provides a less expensive and simpler method for precise tumor resection [111–113].

In recent years, PLNPs have been positively involved in theranostic studies, as PersL can be used to determine the accurate position and time of therapy, allegedly "imaging-guided therapy". Owing to the versatile surface functions of PLNPs, photothermal agents and photosensitizers can be easily loaded onto PLNP nanoplatforms for PersL imaging-guided therapy, demonstrating outstanding advantages in this field. In addition, PLNPs can be excited by different excitation sources, including UV, LED, NIR laser, X-ray and radiopharmaceutical. The application of different excitation sources is helpful for overcoming the problems of poor imaging quality and penetration depth caused by shortwave excitation [114]. From multiple perspectives, the manufacturing of PLNPs based nanoprobes for biological applications should follow the following standards: (i) strong and stable initial luminescence, long afterglow, and repeatable regeneration; (ii) suitable size for in vivo applications (< 200 nm); (iii) Target trigger signal changes for biosensing; (iv) The passive or active targeting ability of biological imaging; (v) The specific multifunctionality of therapeutics [29, 44, 115]. In 2011, Sun et al. prepared PLNPs nanoprobe based on target-induced FRET system interruption for the detection of α-fetal protein (Fig. 11) [116]. PLNPs are also suitable for fluorescence-guided surgery. For example, in 2019, Ni et al. synthesized a NIR afterglow luminescent nanoparticle with aggregation-induced emission (AIE) characteristics of rapid PersL signal quenching in normal tissues and an ultrahigh tumor-to-liver signal ratio [117]. These fascinating features make AIE PLNPs excellent imaging-guided probes for the resection of peritoneal cancer. In 2018, Tian et al. used $ZnGa_2O_4:Cr^{3+}$ for long-term image-guided surgery of hepatocellular carcinoma (HCC). Interestingly, $ZnGa_2O_4:Cr^{3+}$ can be taken up by normal liver tissue but not by HCC tumor tissue, allowing for precise localization after more radical resection [118]. These findings indicate that PLNPs can further contribute to areas such as the study of complex molecular networks and the construction of guiding systems for surgery.

In addition, in contrast to traditional fluorescent agents such as semiconductor quantum dots, upconversion nanoparticles, and organic dyes, the optical imaging of PLNPs can eliminate real-time excitation from external light sources, completely avoiding interference from their own fluorescence and achieving high sensitivity in vivo imaging. In 2023, Lin et al. constructed mZGS@Mn-AMD, an image-guided tumor resection. The MnO_2 shell quenches PersL in normal tissue and is degraded in the TME. Owing to the improved sensitivity of tumor imaging, multiple types of residual tumor tissue can be successfully recognized via PersL imaging [119].

Table 4 Comparison of the mechanism of PLNPs in PDT/PTT

Year	PLNPs	Surface coating	Excitation	Emission wavelength (nm)	PersL duration	Mechanism	Application	References
2017	$Zn_{1.25}Ga_{1.5}Ge_{0.25}O_4$:0.5% Cr^{3+}, 2.5% Yb^{3+}, and 0.25% Er^{3+}	Mesoporous silica layers and aluminum phthalocyanine (AlPcS)	405 nm UV laser	690 nm	20 min	ROS generated by AlPcS via the FRET process	PersL bioimaging and PDT in vivo	[23]
2016	$Zn_3Ga_4Ge_2O_{13}$:0.3%Cr^{3+}	Si-Pc	808 nm NIR laser	694 nm	4 h	The overlap of the PersL spectra of PLNPs and the absorption spectra of Si-Pc provides a probability to generate $^1O_2$	Long-term PDT effect in vivo	[106]
2017	$ZnGa_{1.996}O_4$:$Cr_{0.004}$)	2-(1-hexyloxyethyl)-2-devinyl pyropheophorbide-α (HPPH)	White LED	695 nm	10 min	Activation of HPPH with NIR PersL to produce $^1O_2$ based on the spectral overlap between the absorption of HPPH and the PersL emission of PLNPs	Repeatable NIR PersL-excited PDT	[107]
2017	$ZnGa_2O_4$:Cr^{3+}	MSNs and ICG	226 nm UV laser	696 nm	1 h	ICG@mZGC as the drug delivery system delivers and releases ICG into tumor cells, and generate heat to kill tumor cells under 808 nm laser irradiation	Bioimaging& PTT in vitro and in vivo irradiated by continuous 808 laser	[108]
2021	$ZnGa_2O_4$: Cr	PDA and DOX	254 nm UV laser	508&714 nm	1 h	Photothermal effect of PDA under irradiation speeded up the release of DOX to enhance the antitumor effects and reduce the side effects of the drugs	Chemo-PTT synergetic therapeutic effects	[109]
2020	$Zn_{1.25}$ Ga, $_{1.5}$Ge, $_{0.25}O_4$: 0.5%Cr^{3+}, 2.5%Yb^{3+}, 0.25%Er^{3+}	BAC and PEG	254 nm UVlaser	695 nm	4 h	NIR-emitting PLNPs as a built-in excitation source for continuous external irradiation-free imaging and phototherapy	Cell targeting NIR imaging and PTT/PDT In vivo	[110]

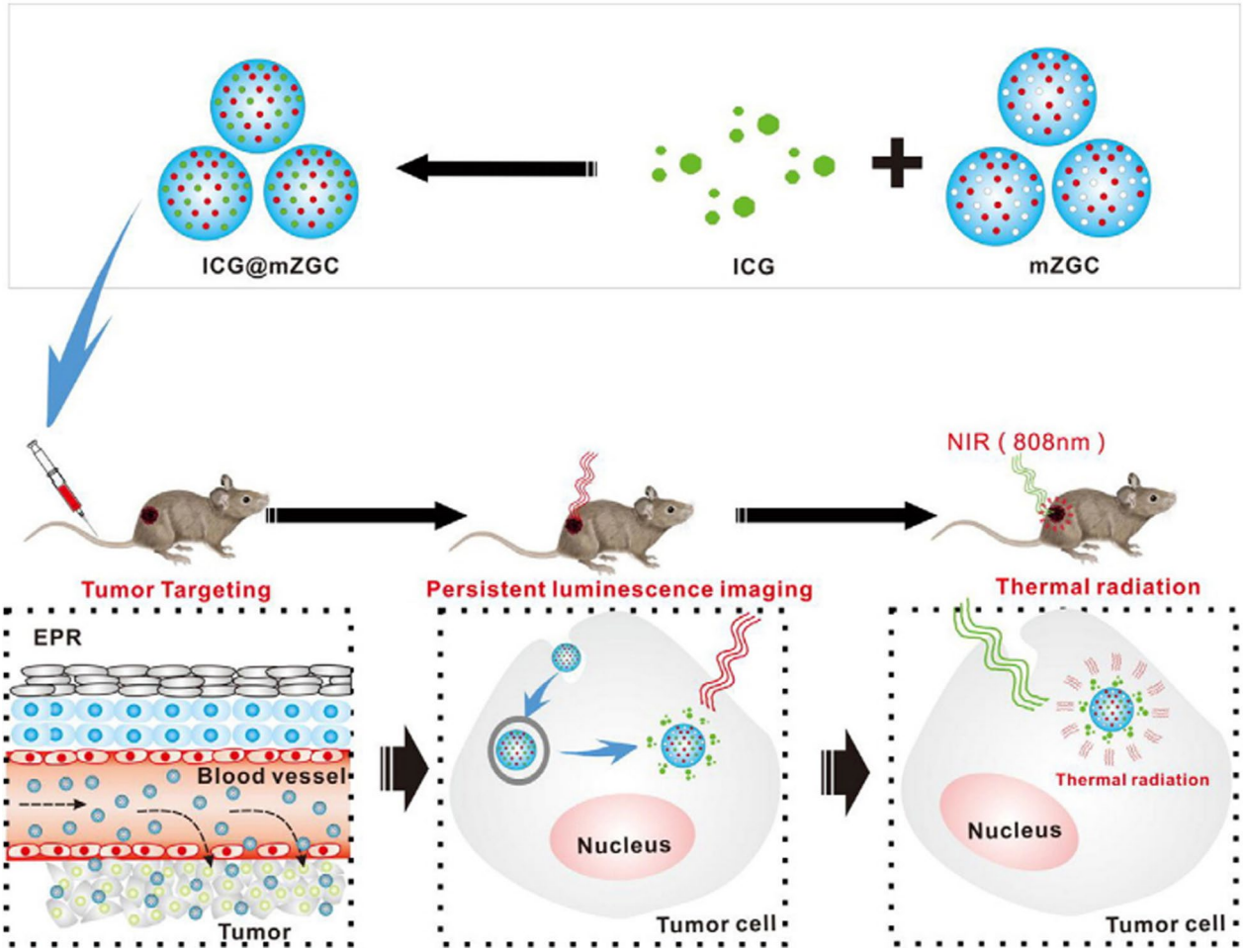

Fig. 10 A schematic illustration shows applications of the NPs for persistent luminescent imaging-guided PTT in vivo. In this schematic illustration, the ICG and PersL phosphors co-loaded mesoporous silica nanoparticle. Reproduced with permission [108]. Copyright 2017, Elsevier

Targeted anti-tumor drug delivery based on PLNPs

Chemotherapy is widely used in clinical cancer treatment, but its poor targeting ability can result in severe toxic side effects, such as dose-limiting side effects. The clinical manifestations of chemotherapy-induced peripheral neuropathy include pain, numbness, proprioceptive deficits, muscle weakness, falls, dizziness, headache, and even paralysis [120]. Fortunately, PLNPs have been integrated into various drug delivery systems to achieve precise drug release and real-time monitoring, avoiding dose-dependent side effects.

Liposomes have been extensively used as nanocarriers owing to their excellent biocompatibility, low toxicity and biodegradability.

In 2017, Yan et al. used liposome-coated PLNPs as carriers of the drug paclitaxel (PTX) to inhibit the growth of human breast cancer (MCF-7) with simultaneous luminescence signals [121]. MSNs give PLNPs an easy-to-modify surface, which allows PLNPs to bind with various functional molecules, metal nanomaterials and cell membranes, which enables the excellent targeting ability and immune escape of PLNPs. MSNs with high pore volume are another commonly used drug carrier. A Lipo-PLNP-PTX nano-system constructed on the basis of this mechanism achieved an ideal PTX encapsulation efficiency as high as 69.2%, with excellent PTX release. Lipo-PLNP-PTX achieved a high PTX release efficiency of 98.9% within 24 h in 50% human serum, while the drug release rate of Lipo-PLNP-PTX in PBS at 4 °C was only 10.5%, which indicates the good stability of Lipo-PLNP-PTX under storage conditions. Richard et al. embedded $ZnGa_{1.995}Cr_{0.005}O_4$ PLNPs in an MSN shell and then loaded them with the antitumor drug DOX. This drug-loaded probe can release DOX in a pH-sensitive manner, and its distribution can be easily monitored in vivo [122]. To further improve the targeting ability, Yan et al. conjugated the pH-low-insertion peptide to MSN-coated PLNPs via the GFLG peptide and disulfide bonds to

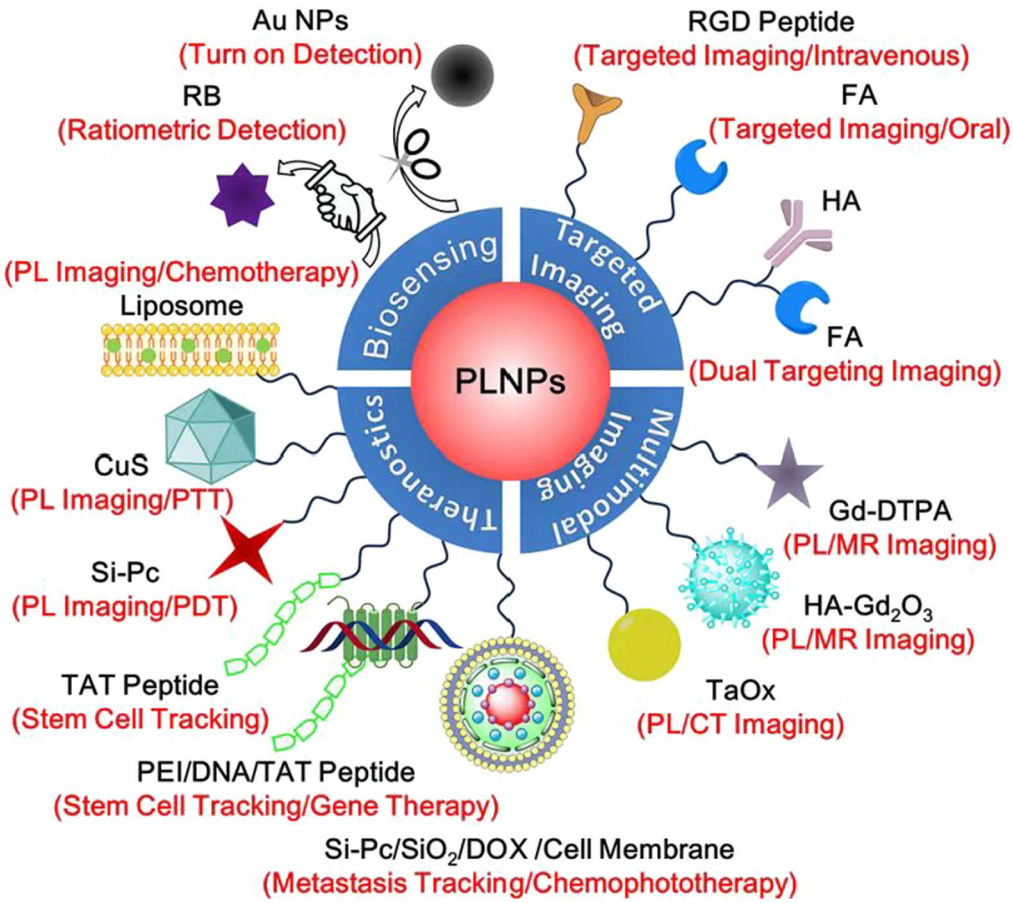

Fig. 11 Engineering strategies of PLNPs for biological applications. Reproduced with permission [116]. Copyright 2018, American Chemical Society

target the acidic tumor microenvironment. In addition, GFLG and disulfide bonds are two switches that can be specifically opened by highly expressed CB and GSH in tumor cells. Because of this principle, the MSPLNPs triggered the release of loaded DOX in a PBS solution containing CB and GSH, achieving a drug release efficiency of more than 90% within 8 h to effectively inhibit the growth of tumors [123].

In 2019, Wang et al. synthesized MSN-coated zinc gallogermanate PLNPs to load the colorectal cancer chemotherapeutic drug 5-FU and then coated them with *Lactobacillus reuteri* biofilms, which helped target the colorectum tumor and prevent the digestion of gastric acid [124]. Moreover, the porous framework ZIF-8 also shows great potential as a carrier for anti-tumor drugs. In 2019, Zhao et al. prepared PLNP@ZIF-8 via a surface adsorption-induced self-assembly strategy, which presented a high DOX loading capacity. More importantly, the acidic tumor microenvironment activated the disassembly of ZIF-8, thus promoting DOX release and enhancing the luminescence of the PLNPs [65].

Synergistic effects of imaging and therapy based on PLNPs

Combination of PLNPs imaging and PDT application

Many studies have investigated the application of PLNPs in tumor imaging and antitumor therapy. In addition, the combination of the performance of PLNPs in imaging and PDT-induced tumor killing has been used to achieve ideal tumor diagnosis and treatment effects. In 2017, Chen et al. used hydrothermal method to prepare $LiGa_5O_8$: Cr (LGO: Cr) PLNPs, which were combined with the photosensitizers 2,3-naphthalocyanine (NC) and mesoporous silica nanoparticles to obtain NC-LGO: Cr@mSiO_2 [125]. Under X-ray excitation, NC-LGO: Cr@mSiO_2 exhibited 2 h of NIR-PersL excitation with a penetration depth more than 1.5 cm. In vivo, long-term repeatable imaging in nude mice was confirmed. The overlap of the excitation wavelengths of the NCs and the emission wavelengths of LGO: Cr caused the material to generate $^1O_2$ under X-ray excitation, thus realizing the effective killing of H1299 human non-small cell lung cancer cells in vitro and the PDT treatment of lung cancer in vivo. In 2020, Shi et al. combined tin-doped

ZGSPLNPs with the photosensitizer $ZnPC_4$ to prepare NIR-PersL $ZnPcS_4$ [126]. It showed an ideal imaging function for deep tissues in vivo and could induce $ZnPC_4$ to produce $^1O_2$ under the excitation of a 659 nm LED, suggesting the construction of an excellent NP system for killing tumors by combining deep imaging with PDT.

Combined application of PLNPs imaging and chemotherapy

In addition to PDT applications, research on the combination of chemotherapy and PLNPs imaging has made remarkable progress. In 2019, Su et al. modified $Zn_{1.1}Ga_{1.8}Ge_{0.1}O_4$:0.5%$Cr^{3+}$, 0.5%$Eu^{3+}$ PLNPs with dopamine (PDA), polyethyleneimine (PEI), folic acid (FA) and doxorubicin (DOX) and realized siRNA loading [127]. The prepared PPP-FA-DOX-siRNA could target the DOX-resistant human breast cancer cell line MCF-7 in vitro and effectively release DOX in an acidic environment. They effectively killed tumor cells via PTT under irradiation with an 808 nm laser, thus realizing the triple collaborative diagnosis and treatment of targeted imaging labeling, drug delivery and PTT. In 2021, Zou et al. prepared NIR-PersL $ZnGa_2O_4$:Cr^{3+}, Sn^{4+} PLNPs via the template method and modified them with mesoporous silica, DOX and PEG [128]. The DOX-Mn-ZGOCS-PEG had good imaging ability for tumor-specific external magnetic resonance (MR) in vivo and in vitro and achieved excellent DOX release and anticancer effects in the tumor microenvironment, thus achieving effective chemotherapy under the guidance of tumor microenvironment-targeted MR/NIR-PersL imaging.

Future perspectives

This review summarizes the synthesis, modification and research progress of PLNP in targeted tumor imaging and tumor killing (Table 5). At present, some progress has been made in the application of PLNPs in targeted biological imaging and killing of tumors, but many aspects of further research are needed in the future.

Perspectives in the synthesis and modification of PLNPs

This review first explains the necessity of synthesizing nanoscale PLNPs for antitumor applications and the advantages of high imaging sensitivity and ease of surface functionalization over micrometer-sized PLNPs. The three main methods used to prepare PLNPs include the sol–gel method, the precisely controlled templated method, and surface modification, which is a convenient hydrothermal method. Surface functionalization plays a pivotal role in enhancing the biocompatibility and functionality of PLNPs. Coatings of mesoporous silica or PAA/CaP shells improve stability and enable targeted therapeutic applications. Additionally, PANI/GCS grafting creates pH-responsive platforms for precise biomedical imaging and therapy, and the integration of multiple modification strategies promises to further enhance the functionality of PLNPs. As a result, in terms of antitumor applications, PLNPs are used as optical carriers to track cancer cells, graft functional groups with antitumor effects, and undergo surface modification by coatings such as PDA, liposomes, and silica. Thus, nanosystems with long-lasting bioimaging and anti-tumor effects were obtained. In addition, various tumor markers, mainly immune checkpoint inhibitors of PD-1, have been utilized as effective tumor targets. However, continued research into advanced synthesis and surface functionalization methods will drive the development of PLNPs for increasingly sophisticated biomedical applications, including imaging, therapy, and theranostics.

Despite significant progress in the synthesis of PLNPs, there are still some issues with the morphological regulation of PLNPs. In terms of biomedical applications, more advanced synthesis methods are needed to precisely control the morphology, particle size, surface properties, PersL strength, and PersL time of PLNPs, in order to construct PLNPs nanoplatform with high-efficiency [129]. Synthesizing PLNP materials with uniform structures can enhance the active region of the sensing interface, and the use of microfluidic platforms with advantages such as high throughput and reproducibility may provide a superior solution to these challenges. In addition to the co-synthesis method, which combines several synthesis methods, the synthesized PLNPs also combine the advantages of various synthesis methods in terms of properties such as afterglow properties, particle size, and morphological aspects. This also provides a solution for synthesizing PLNPs with balanced properties. BesidesIn addition, EDTA etching of sintered PLNPs can effectively reduce their size and greatly improve water dispersion. Microwave-assisted heating effectively improves the efficiency of PLNPs synthesis, and the emergence of organic PLNPs also makes them promising for biomedical applications. However, problems such as the serious spin-forbidden barrier between single and triplet excited states and the serious non-radiative leaps of excitons in triplet states still seriously hinder the development of organic PLNPs, and researchers are gradually exploring the prospects of organic PLNPs through the introduction of heavy atoms, crystal engineering and other strategies.

Perspectives in the optical properties and tumor imaging application of PLNPs

PLNPs avoid tissue autofluorescence and greatly improve the SNR, which has attracted great attention in tumor imaging. Considering the short afterglow time of UV preexcitation and the short penetration depth of visible

Table 5 Comparison of PersL duration and Application of PLNPs

	Year	PLNPs	Excitation wavelength (nm)	Emission wavelength (nm)	PersL duration	Application	References
Tumor imaging of PLNPs in vitro	2022	Zn@SiNSs	365 nm	510 nm	200 min	Imaging of live U87MG human glioblastoma cells	[88]
Tumor imaging of PLNPs in vivo	2020	$ZnGa_{1.995}Cr_{0.005}O_4$	365 nm	697 nm	10 min	Tumor imaging in vivo	[97]
	2013	$Zn_{2.94}Ga_{1.96}Ge_2O_{10}:Cr^{3+},Pr^{3+}$	254 nm	695 nm	15 days	Long-term targeted tumor imaging in vivo	[55]
Tumor imaging of PLNPs in vivo and in vitro	2020	$Zn_{1.1}Ga_{1.8}G_{e0.1}O_4:Eu_{0.009}$, $Cr_{0.09}$	410 nm	698 nm	10 min	Long-term tracking of MDA-MB-231 metastatic breast cancer cells in vitro & tumor metastasis in vivo	[70]
	2016	$ZnGa_2O_4$:Cr,B	254 nm	700 nm	3 days	Imaging of MCF-7 breast cancer cells in vitro & persistent tumor-bearing mice in vivo	[89]
PDT	2016	$Zn_3Ga_4Ge_2O_{13}:0.3\%Cr^{3+}$	808 nm	694 nm	4 h	Persistent luminescence sensitized PDT effect in vivo	[106]
	2017	$ZnGa_{1.996}O_4:Cr_{0.004}$)	White LED	695 nm	10 min	Repeatable NIR PersL-excited PDT	[107]
PTT	2017	ICG@Mzgc $ZnGa_2O_4:Cr^{3+}$	226 nm	696 nm	1 h	PTT in vitro and in vivo	[108]
	2021	$ZnGa_2O_4$: Cr	254 nm	508&714 nm	1 h	Chemo-PTT synergetic therapeutic effects	[109]
PDT&PTT	2020	$Zn_{1.25}$ Ga, $_{1.5}$Ge, $_{0.25}O_4$: $0.5\%Cr^{3+}$, $2.5\%Yb^{3+}$, $0.25\%Er^{3+}$	254 nm	695 nm	4 h	Cell targeting NIR imaging and PTT/PDT in vivo	[110]
Fluorescence-guided surgery	2018	$ZnGa_2O_4Cr_{0.004}$	254 nm	696 nm	5 h	Luminescence imaging guidance during HCC operation	[118]
	2023	$Zn_{1.3}Ga_{1.4}Sn_{0.3}O_4:Cr_{0.005}$, $Y_{0.003}$	659 nm	702 nm	30 min	Ultrasensitive PLNPs nanoprobe to guide surgical removal	[119]
Drug delivery	2017	$Zn_{1.1}$ Ga-PTX, $_{1.8}$Ge, $_{0.1}$, O_4: Cr^{3+}	650 nm	695 nm	5 min	Long-term bioimaging in vivo & high PTX loading efficiency	[121]
	2019	$Zn_{1.1}Ga_{1.8}Ge_{0.1}O_4:0.5\%Cr^{3+}$,0 .5%$Eu^{3+}$	254 nm	695 nm	6 h	pH-driven targeting DOX release for persistent luminescence imaging-guided chemotherapy	[123]
	2019	$Zn_{1.25}Ga_{1.5}Ge_{0.25}O_4:0.5\%Cr^{3+}$, $2.5\%Yb^{3+}$, $0.25\%Er^{3+}$	254 nm	696 nm	30 min	Persistent luminescence bioimaging & targeted delivery of oral drugs into the colorectum for colorectal cancer treatment	[124]

light, increasing research has focused on NIR and X-ray excitation. NIR light results in improved deep tissue permeation and reduced photodamage, and it can release precharged energy in deep traps to achieve reactivation. However, during the NIR-recharging process of carrier redistribution from deeper traps to shallower traps, the depletion of carriers leads to decreased afterglow intensity. By creating "upconversion-like" trap-energy storage, carriers can be captured first by deep traps and then transferred to shallow traps, and such opposite energy transfer can result in more stable persistent luminescence [130]. To achieve repeated charging, novel systems

should be designed to pump carriers from the luminescent center into shallow traps under NIR excitation. X-rays have also been used as an excitation source for deep penetration, but the radiation dose of X-rays must be carefully set to avoid potential safety risks. Radiopharmaceuticals such as 18F-fluorodeoxyglucose can efficiently excite fluorescence and afterglow luminescence via Cerenkov resonance energy transfer and ionizing radiation. Combining tumor-selective radiopharmaceuticals with PLNPs can provide a new way to image tumors with high sensitivity and long decay times.

To obtain novel PLNP materials with higher excitation efficiency and better PersL properties, future studies should focus on improving the response efficiency to red light, NIR light, and X-rays. Finally, although imaging with novel PLNP materials has high sensitivity, it cannot provide all the information needed for disease diagnosis. Therefore, it is necessary to combine these methods with other imaging modalities to provide more accurate and reliable information. In addition, the development of highly hydrophilic PLNPs that can target specific tissues or tumor cells through ligand modification represents a significant advancement in noninvasive and long-term in vivo imaging. This evolution from UV to NIR luminescence, along with the ability to reactivate PersL without continuous excitation, opens new avenues for safer and more effective imaging techniques that could greatly benefit medical diagnostics and research.

Design of multifunctional PLNPs with excellent tumor-killing potential for clinical application

In addition, in anti-tumor research, PLNPs have advantages such as ideal optical performance, PersL after removing excitation light and the exclusion of background fluorescence interference from in situ excitation. PLNPs also provide good antitumor performance via PTT, PDT, surgery, drug delivery, and other methods, with great progress in related fields. However, these methods also have certain limitations and need further research. First, most studies on the biocompatibility of PLNPs are based on the cytotoxicity level, and the elimination of toxic side effects on normal tissues at the gene, protein, and metabolic levels still needs to be verified. Second, PLNPs have superior optical performance, but the diagnostic information provided by imaging with PLNPs is limited, and the migration, transformation, and distribution of PLNPs during in vivo imaging still need to be studied. Hopefully, more studies could be conducted to develop PLNPs with excellent optic properties and explore their wide application in tumor diagnosis and treatment. In addition, the role of PLNPs in PTT and PDT therapy is usually to provide light excitation for photosensitizers. There are relatively few reports on the ability of PLNPs to generate ROS or heat energy under photoexcitation. Therefore, current nanomaterial systems based on PLNPs rely heavily on the performance of the photosensitizer to achieve PDT and PTT. Moreover, upconversion PLNPs, which emit high-energy light under low-energy light excitation conditions, exhibit superior deep tissue penetration ability [131, 132]. However, these methods are lacking in tumor imaging and treatment reports; thus, further research is urgently needed. In summary, tumor-targeted bioimaging and killing materials based on PLNPs are making rapid progress, but there is still much room for improvement in the preparation of this emerging field. It is hoped that PLNPs related materials can be further developed for precise and effective treatment of cancer in the future.

Current research on near-infrared PLNPs in the field of tumor imaging and therapy is promising but still faces multiple challenges. Limitations in material properties are the primary issue, as most PLNPs have a narrow dynamic range of afterglow signals. In addition, traditional PLNPs rely on in vitro UV excitation, making it difficult to achieve in vivo in situ cyclic charging, and the emission wavelengths of existing materials are mostly concentrated in the NIR-I window (650–950 nm), which still has a limited penetrating imaging effect on deep tumors. In terms of synthesis and biological application, inorganic PLNPs are complicated to synthesize and prone to large particles, whereas organic PLNPs can be tailored to the active site but have poor stability and low afterglow efficiency. Moreover, most PLNPs lack specific targeting modifications and rely on passive enrichment, whereas surface modifications may interfere with luminescence performance or trigger an immune response. Finally, the difficulty of integrating multimodal therapeutics further restricts their development: existing studies focus on a single function (e.g., long afterglow imaging or PTT/PDT) and lack the synergistic design of therapeutic integration, and the long-term toxicity, metabolic pathway, and standards for large-scale production of PLNPs have yet to be clarified, which leads to a significant barrier to clinical translation.

To address the aforementioned challenges, future studies should break through conventional paradigms and pursue interdisciplinary integration. The AI-guided design of PLNPs represents a critical direction of machine learning models; for example, generative adversarial networks can predict rare-earth ion doping ratios and surface modification schemes to optimize afterglow intensity and emission wavelengths. By integrating tumor-specific metabolic profiles (e.g., glycolytic activity), AI-driven platforms may further enable the customization of pH-responsive or enzyme-activated PLNPs

while dynamically adjusting photothermal therapy parameters.

Another strategic breakthrough lies in multimodal theranostic platforms. For example, Wu et al. demonstrated the integration of long-afterglow materials with polypyrrole for dual-modal afterglow/photoacoustic imaging and photothermal therapy in breast cancer [133].

In situ self-energizing technologies could minimize the reliance on external excitation sources. Inspired by "wormhole-inspired" material design, in vivo cyclic recharging of PLNPs can be achieved via low-energy near-infrared light (740 nm) [130]. Concurrently, leveraging Fenton-like reactions to harness tumor microenvironment metabolites (e.g., H_2O_2) as excitation energy sources for PLNPs may increase the energy conversion efficiency.

Finally, advancing is imperative. Green synthesis approaches such as aqueous-phase reactions, clinical translation and standardization of o-templated protocols could reduce production costs. Coupling metabolomics with immunohistochemical profiling to establish comprehensive long-term toxicity evaluation frameworks will accelerate the transition to clinical trials.

Conclusion

In summary, PLNPs have been used for tumor-targeted imaging and killing, showing great application prospects in the field of tumor diagnosis and treatment. In terms of imaging, PLNPs have shown an ideal imaging effect and low degree of radiation damage, which is obviously superior to traditional tumor diagnosis methods, while avoiding the in situ excitation interference of commonly used fluorescent nanoimaging materials. Among them, NIR-emitting PLNPs show excellent penetration depth. In terms of tumor killing, PLNPs have achieved outstanding antitumor effects via PDT, PPT, FGS, drug delivery and their combined application. However, further modifications, the preparation of safer and more effective imaging PLNPs and the design of multifunctional PLNPs with excellent tumor killing potential for clinical application still need further study. It is hoped that more efforts will be made in the future to develop PLNPs with excellent imaging performance and explore their wide application in tumor diagnosis and treatment.

Acknowledgements
We thanks professor Yuhua Wang from School of Materials and Energy, Lanzhou University for his kindly help in the design of this paper (No. lzukqky-2023-t07).

Author contributions
R Tan, and J Wu contributed equally. P Zhou, Y Sun, R Tan, and J Wu contributed to designing the study and critically revised the manuscript. R Tan, J Wu, C Wang, Z Zhao, Z Zhang, C Zhong, Z Tang, R Zheng, B Du and Y He contributed to the drafting and review of the manuscript. All the authors have read and approved the article and have due diligence to ensure the integrity of the manuscript. Neither the entire manuscript nor any part of its content has been published or accepted elsewhere.

Funding
This research received funding from the Natural Science Foundation of Gansu Province (No. 22YF7FA017), the Fundamental Research Funds for the Central Universities (No. lzujbky-2021-ey14, lzujbky-2022-kb03), the Gansu Province Health Industry Research Project (No. GSWSKY2023-70), the Joint Research Fund of Gansu Province (No. 24JRRA945, 24JRRA948), the CSA West China Clinical Research Fund (No. CSA-W2024-11), the Lanzhou University Hospital of Stomatology Research Support Fund (No. lzukqky-2023-t07), the Lanzhou University Innovation and Entrepreneurship Cultivation Project, the Medical Innovation and Development Project of Lanzhou University, and the Open Subject Foundation of the Key Laboratory of Dental Maxillofacial Reconstruction and Biological Intelligence Manufacturing.

Data availability
No datasets were generated or analysed during the current study.

Declarations

Ethics approval and consent to participate
Not applicable.

Consent for publication
All the authors have read and approved the manuscript.

Competing interest
The authors declare no competing interests.

Author details
[1]School and Hospital of Stomatology, Key Laboratory of Dental Maxillofacial Reconstruction & Biological Intelligence Manufacturing of Gansu Province, Lanzhou University, Lanzhou 730000, People's Republic of China. [2]School of Physical Science and Technology, Lanzhou University, Lanzhou 730000, People's Republic of China. [3]School of Stomatology, Xuzhou Medical University, Xuzhou 221000, People's Republic of China. [4]Department of Stomatology, the Affiliated Hospital of Xuzhou Medical University, Xuzhou 221000, People's Republic of China.

Received: 27 January 2025 Accepted: 23 March 2025
Published online: 17 April 2025

References

1. Lozano R, Naghavi M, Foreman K, Lim S, Shibuya K, Aboyans V, Abraham J, Adair T, Aggarwal R, Ahn SY, et al. Global and regional mortality from 235 causes of death for 20 age groups in 1990 and 2010: a systematic analysis for the Global Burden of Disease Study 2010. Lancet. 2012;380:2095–128.
2. Dolmans DE, Fukumura D, Jain RK. Photodynamic therapy for cancer. Nat Rev Cancer. 2003;3:380–7.
3. Castano AP, Mroz P, Hamblin MR. Photodynamic therapy and anti-tumour immunity. Nat Rev Cancer. 2006;6:535–45.
4. Yun SH, Kwok SJJ. Light in diagnosis, therapy and surgery. Nat Biomed Eng. 2017;1.
5. Engbersen MP, Van Driel W, Lambregts D, Lahaye M. The role of CT, PET-CT, and MRI in ovarian cancer. Br J Radiol. 2021;94:20210117.
6. Lother D, Robert M, Elwood E, Smith S, Tunariu N, Johnston SRD, Parton M, Bhaludin B, Millard T, Downey K, et al. Imaging in metastatic breast cancer, CT, PET/CT, MRI, WB-DWI, CCA: review and new perspectives. Cancer Imaging. 2023;23:53.
7. Liu Y, Chen C, Liu L, Li Y. Comparison of MRI and CT scan for the detection of liver cancer. Curr Med Imaging. 2023;19:995–1004.
8. Yamada Y, Okawa S. Diffuse optical tomography: present status and its future. Opt Rev. 2014;21:185–205.
9. Richardson JC, Bowtell RW, Mäder K, Melia CD. Pharmaceutical applications of magnetic resonance imaging (MRI). Adv Drug Deliv Rev. 2005;57:1191–209.

10. Bateman TM. Advantages and disadvantages of PET and SPECT in a busy clinical practice. J Nucl Cardiol. 2012;19(Suppl 1):S3-11.
11. de Jong M, Essers J, van Weerden WM. Imaging preclinical tumour models: improving translational power. Nat Rev Cancer. 2014;14:481–93.
12. Wang S, Ren WX, Hou JT, Won M, An J, Chen X, Shu J, Kim JS. Fluorescence imaging of pathophysiological microenvironments. Chem Soc Rev. 2021;50:8887–902.
13. Hu X, Zhu Z, Dong H, Zhu X, Zhu H, Ogawa K, Odani A, Koh K, Chen H. Inorganic and metal-organic nanocomposites for cascade-responsive imaging and photochemical synergistic effects. Inorg Chem. 2020;59:4617–25.
14. Zhang J, Liu J, Niu C, Wu Q, Tan J, Jing N, Wen Y. Functionalized fluorescent organic nanoparticles based AIE enabling effectively targeting cancer cell imaging. ChemBioChem. 2023;24:e202300391.
15. Sun ZF, Chang Y, Xia N. Recent development of nanomaterials-based cytosensors for the detection of circulating tumor cells. Biosensors (Basel). 2021;11:281.
16. Pirsaheb M, Mohammadi S, Salimi A, Payandeh M. Functionalized fluorescent carbon nanostructures for targeted imaging of cancer cells: a review. Mikrochim Acta. 2019;186:231.
17. Zhou N, Hao Z, Zhao X, Maharjan S, Zhu S, Song Y, Yang B, Lu L. A novel fluorescent retrograde neural tracer: cholera toxin B conjugated carbon dots. Nanoscale. 2015;7:15635–42.
18. Wang C, Chen L, Tan R, Li Y, Zhao Y, Liao L, Ge Z, Ding C, Xing Z, Zhou P. Carbon dots and composite materials with excellent performances in cancer-targeted bioimaging and killing: a review. Nanomedicine (Lond). 2023;2023:0216.
19. Kesharwani P, Ma R, Sang L, Fatima M, Sheikh A, Abourehab MAS, Gupta N, Chen ZS, Zhou Y. Gold nanoparticles and gold nanorods in the landscape of cancer therapy. Mol Cancer. 2023;22:98.
20. Xu J, Ning J, Wang Y, Xu M, Yi C, Yan F. Carbon dots as a promising therapeutic approach for combating cancer. Bioorg Med Chem. 2022;72: 116987.
21. Maldiney T, Bessière A, Seguin J, Teston E, Sharma SK, Viana B, Bos AJ, Dorenbos P, Bessodes M, Gourier D, et al. The in vivo activation of persistent nanophosphors for optical imaging of vascularization, tumours and grafted cells. Nat Mater. 2014;13:418–26.
22. Wu S, Li Y, Ding W, Xu L, Ma Y, Zhang L. Recent advances of persistent luminescence nanoparticles in bioapplications. Nanomicro Lett. 2020;12:70.
23. Wang J, Li Y, Mao R, Wang Y, Yan X, Liu J. Persistent luminescent nanoparticles as energy mediators for enhanced photodynamic therapy with fractionated irradiation. J Mater Chem B. 2017;5:5793–805.
24. Kumar V, Bhatt D, Saruchi PS. Luminescence nanomaterials for biosensing applications. Luminescence. 2023;38:1011–25.
25. Liu Y, Li J, Xiahou J, Liu Z. Recent advances in NIR or X-ray excited persistent luminescent materials for deep bioimaging. J Fluoresc. 2023;1:179–95.
26. Liang L, Chen N, Jia YY, Ma QQ, Wang J, Yuan Q, Tan WH. Recent progress in engineering near-infrared persistent luminescence nanoprobes for time-resolved biosensing/bioimaging. Nano Res. 2019;12:1279–92.
27. Pei P, Chen Y, Sun C, Fan Y, Yang Y, Liu X, Lu L, Zhao M, Zhang H, Zhao D, et al. X-ray-activated persistent luminescence nanomaterials for NIR-II imaging. Nat Nanotechnol. 2021;16:1011–8.
28. Liu N, Chen X, Sun X, Sun X, Shi J. Persistent luminescence nanoparticles for cancer theranostics application. J Nanobiotechnology. 2021;19:113.
29. Li Y, Gecevicius M, Qiu J. Long persistent phosphors–from fundamentals to applications. Chem Soc Rev. 2016;45:2090–136.
30. le Masne de Chermont Q, Chaneac C, Seguin J, Pelle F, Maitrejean S, Jolivet JP, Gourier D, Bessodes M, Scherman D. Nanoprobes with near-infrared persistent luminescence for in vivo imaging. Proc Natl Acad Sci USA 2007;104:9266–71.
31. Li Z, Zhang Y, Wu X, Wu X, Maudgal R, Zhang H, Han G. In vivo repeatedly charging near-infrared-emitting mesoporous SiO(2)/ZnGa(2)O(4):Cr(3+) persistent luminescence nanocomposites. Adv Sci (Weinh). 2015;2:1500001.
32. Wang J, Li J, Yu J, Zhang H, Zhang B. Large hollow cavity luminous nanoparticles with near-infrared persistent luminescence and tunable sizes for tumor afterglow imaging and chemo-/photodynamic therapies. ACS Nano. 2018;12:4246–58.
33. Li Z, Zhang Y, Wu X, Huang L, Li D, Fan W, Han G. direct aqueous-phase synthesis of sub-10 nm "luminous pearls" with enhanced in vivo renewable near-infrared persistent luminescence. J Am Chem Soc. 2015;137:5304–7.
34. Wang J, Ma Q, Hu XX, Liu H, Zheng W, Chen X, Yuan Q, Tan W. Autofluorescence-free targeted tumor imaging based on luminous nanoparticles with composition-dependent size and persistent luminescence. ACS Nano. 2017;11:8010–7.
35. Wang HF, Chen X, Feng F, Ji X, Zhang Y. EDTA etching: a simple way for regulating the traps, size and aqueous-dispersibility of Cr(3+)-doped zinc gallate. Chem Sci. 2018;9:8923–9.
36. Teston E, Richard S, Maldiney T, Lievre N, Wang GY, Motte L, Richard C, Lalatonne Y. Non-aqueous sol-gel synthesis of ultra small persistent luminescence nanoparticles for near-infrared in vivo imaging. Chemistry. 2015;21:7350–4.
37. Yang X, Waterhouse GIN, Lu S, Yu J. Recent advances in the design of afterglow materials: mechanisms, structural regulation strategies and applications. Chem Soc Rev. 2023;52:8005–58.
38. Yan LX, Wang BB, Zhao X, Chen LJ, Yan XP. A pH-responsive persistent luminescence nanozyme for selective imaging and killing of helicobacter pylori and common resistant bacteria. ACS Appl Mater Interfaces. 2021;13:60955–65.
39. Fu X, Zhao X, Chen LJ, Ma P, Liu T, Yan XP. Mesoporous polyacrylic acid/calcium phosphate coated persistent luminescence nanoparticles for improved afterglow bioimaging and chemotherapy of bacterial infection. Biomater Sci. 2023;11:5186–94.
40. Yan LX, Chen LJ, Zhao X, Yan XP. pH switchable nanoplatform for in vivo persistent luminescence imaging and precise photothermal therapy of bacterial infection. Adv Funct Mater. 2020;30:12.
41. Li Y, Teng X, Wang Y, Yang C, Yan X, Li J. Neutrophil delivered hollow titania covered persistent luminescent nanosensitizer for ultrosound augmented chemo/immuno glioblastoma therapy. Adv Sci (Weinheim, Ger). 2021;8:e2004381.
42. Zhang Z, Yan H, Cao W, Xie S, Ran P, Wei K, Li X. Ultrasound-chargeable persistent luminescence nanoparticles to generate self-propelled motion and photothermal/NO therapy for synergistic tumor treatment. ACS Nano. 2023;17:16089–106.
43. Lin Y, Hu J, Wu L, Zou Q, Chen D, Huang D, Lu H, Wang SB, Zhu H. Multiple emission bands NIR-persistent luminescence mSiO(2)@Zn(0.6)Ca(0.4)Ga(2)O(4):Cr(3+), Yb(3+) nanoparticles for biological applications. J Mater Chem B. 2021;9:1131–7.
44. Wang J, Ma Q, Wang Y, Shen H, Yuan Q. Recent progress in biomedical applications of persistent luminescence nanoparticles. Nanoscale. 2017;9:6204–18.
45. Lin Q, Li Z, Ji C, Yuan Q. Electronic structure engineering and biomedical applications of low energy-excited persistent luminescence nanoparticles. Nanoscale Adv. 2020;2:1380–94.
46. Xu J, Tanabe S. Persistent luminescence instead of phosphorescence: history, mechanism, and perspective. J Lumin. 2019;205:581–620.
47. Fritzen DL, Giordano L, Rodrigues LCV, Monteiro J. Opportunities for persistent luminescent nanoparticles in luminescence imaging of biological systems and photodynamic therapy. Nanomaterials. 2020;10:2015.
48. Huang K, Le N, Wang JS, Huang L, Zeng L, Xu WC, Li Z, Li Y, Han G. Designing next generation of persistent luminescence: recent advances in uniform persistent luminescence nanoparticles. Adv Mater. 2022;34:e2107962.
49. Huang K, Dou XJ, Zhang YF, Gao XP, Lin J, Qu JL, Li Y, Huang P, Han G. Enhancing light and X-ray charging in persistent luminescence nanocrystals for orthogonal afterglow anti-counterfeiting. Adv Funct Mater. 2021;31:2009920.
50. Mushtaq U, Ayoub I, Kumar V, Sharma V, Swart HC, Chamanehpour E, Rubahn HG, Mishra YK. Persistent luminescent nanophosphors for applications in cancer theranostics, biomedical, imaging and security. Mater Today Bio. 2023;23:100860.
51. Unnikrishnan B, Wu RS, Wei SC, Huang CC, Chang HT. Fluorescent carbon dots for selective labeling of subcellular organelles. ACS Omega. 2020;5:11248–61.

52. Serge-Correales YE, Neumeyer D, Ullah S, Mauricot R, Zou Q, Ribeiro SJL, Verelst M. Size control and improved aqueous colloidal stability of surface-functionalized ZnGa(2)O(4):Cr(3+) bright persistent luminescent nanoparticles. Langmuir. 2023;39:1495–506.
53. Yang S, Dai W, Tang M, Wang J. Nonstoichiometric nanocubes with a controllable morphology and persistent luminescence for autofluorescence-free biosensing. ACS Appl Mater Interfaces. 2023;15:38644–52.
54. Huang K, Li Z, Li Y, Yu N, Gao X, Huang L, Lim SF, Han G. Three-dimensional colloidal controlled growth of core-shell heterostructured persistent luminescence nanocrystals. Nano Lett. 2021;21:4903–10.
55. Abdukayum A, Chen JT, Zhao Q, Yan XP. Functional near infrared-emitting Cr3+/Pr3+ co-doped zinc gallogermanate persistent luminescent nanoparticles with superlong afterglow for in vivo targeted bioimaging. J Am Chem Soc. 2013;135:14125–33.
56. Wei ZJ, Yin C, Sun M, Long K, Zhang Z, Yan Z, Wang W, Yuan Z. Enhancing persistent luminescence through synergy between optimal electron traps and dye sensitization. ACS Appl Mater Interfaces. 2024;24:531.
57. Xue Z, Li X, Li Y, Jiang M, Liu H, Zeng S, Hao J. X-ray-activated near-infrared persistent luminescent probe for deep-tissue and renewable in vivo bioimaging. ACS Appl Mater Interfaces. 2017;9:22132–42.
58. Song L, Lin X-H, Song X-R, Chen S, Chen X-F, Li J, Yang H-H. Repeatable deep-tissue activation of persistent luminescent nanoparticles by soft X-ray for high sensitivity long-term in vivo bioimaging. Nanoscale. 2017;9:2718–22.
59. Song L, Li PP, Yang W, Lin XH, Liang H, Chen XF, Liu G, Li J, Yang HH. Low-dose X-ray activation of W(VI)-doped persistent luminescence nanoparticles for deep-tissue photodynamic therapy. Adv Funct Mater. 2018;28:10.
60. Qiu X, Zhu X, Xu M, Yuan W, Feng W, Li F. Hybrid nanoclusters for near-infrared to near-infrared upconverted persistent luminescence bioimaging. ACS Appl Mater Interfaces. 2017;9:32583–90.
61. Xiahou J, Zhu Q, Li F, Jin M, Zhu L, Huang S, Zhang T, Sun X, Li J-G. Regulating the trap distribution of ZnGa2O4:Cr3+ by Li+/Ga3+ doping for upconversion-like trap energy transfer NIR persistent luminescence. Inorg Chem Front. 2023;10:2174–88.
62. Chen YF, Spinelli S, Gu ZJ, Pan ZW. Red/NIR/SWIR multi-band persistent probe chargeable by general lighting sources for long-term, high-contrast visible/NIR-I/NIR-II multi-window bioimaging. Chem Eng J. 2022;446:14.
63. Wu L, Hu J, Zou Q, Lin Y, Huang D, Chen D, Lu H, Zhu H. Synthesis and optical properties of a Y(3)(Al/Ga)(5)O(12):Ce(3+), Cr(3+), Nd(3+) persistent luminescence nanophosphor: a promising near-infrared-II nanoprobe for biological applications. Nanoscale. 2020;12:14180–7.
64. Lv M, Zhou W, Tavakoli H, Bautista C, Xia J, Wang Z, Li X. Aptamer-functionalized metal-organic frameworks (MOFs) for biosensing. Biosens Bioelectron. 2021;176:112947.
65. Zhao H, Shu G, Zhu J, Fu Y, Gu Z, Yang D. Persistent luminescent metal-organic frameworks with long-lasting near infrared emission for tumor site activated imaging and drug delivery. Biomaterials. 2019;217:119332.
66. Chen LJ, Zhao X, Liu YY, Yan XP. Macrophage membrane coated persistent luminescence nanoparticle@MOF-derived mesoporous carbon core-shell nanocomposites for autofluorescence-free imaging-guided chemotherapy. J Mater Chem B. 2020;8:8071–83.
67. Shu G, Zhao H, Zhang X. Persistent luminescent metal-organic framework nanocomposite enables autofluorescence-free dual modal imaging-guided drug delivery. Biomater Sci. 2023;11:1797–809.
68. Lv Y, Ding D, Zhuang Y, Feng Y, Shi J, Zhang H, Zhou TL, Chen H, Xie RJ. Chromium-doped zinc gallogermanate@zeolitic imidazolate framework-8: a multifunctional nanoplatform for rechargeable in vivo persistent luminescence imaging and ph-responsive drug release. ACS Appl Mater Interfaces. 2019;11:1907–16.
69. Lin XH, Song L, Chen S, Chen XF, Wei JJ, Li J, Huang G, Yang HH. Kiwifruit-like persistent luminescent nanoparticles with high-performance and in situ activable near-infrared persistent luminescence for long-term in vivo bioimaging. ACS Appl Mater Interfaces. 2017;9:41181–7.
70. Zhao H, Liu C, Gu Z, Dong L, Li F, Yao C, Yang D. Persistent luminescent nanoparticles containing hydrogels for targeted, sustained, and autofluorescence-free tumor metastasis imaging. Nano Lett. 2020;20:252–60.
71. Jiang H, Wang R, Zhang Q, Song L, Sun X, Shi J, Zhang Y. A dual-functional nanoplatform based on NIR and green dual-emissive persistent luminescence nanoparticles for X-ray excited persistent luminescence imaging and photodynamic therapy. Nanoscale. 2022;14:15451–61.
72. Liu X, Xi R, Hu Y, Wang Y, Abdukayum A. A multi-functional nanoplatform based on LiGa(499)O(8):Cr(001)/IrO(2) with near infrared-persistent luminescence, "afterglow" photodynamic and photo-thermal functions. Dalton Trans. 2024;53:6601–8.
73. Liu JM, Zhang DD, Fang GZ, Wang S. Erythrocyte membrane bioinspired near-infrared persistent luminescence nanocarriers for in vivo long-circulating bioimaging and drug delivery. Biomaterials. 2018;165:39–47.
74. Li YJ, Yang CX, Yan XP. Biomimetic persistent luminescent nanoplatform for autofluorescence-free metastasis tracking and chemophotodynamic therapy. Anal Chem. 2018;90:4188–95.
75. Wang J, Li Q, Zhao H, Yue W, Zhang K, Jiang X, Li K. Facile and controllable synthesis of the renal-clearable "luminous pearls" for in vivo afterglow/magnetic resonance imaging. ACS Nano. 2021;16:462–72.
76. Soenen SJ, Rivera-Gil P, Montenegro J-M, Parak WJ, De Smedt SC, Braeckmans K. Cellular toxicity of inorganic nanoparticles: common aspects and guidelines for improved nanotoxicity evaluation. Nano Today. 2011;6:446–65.
77. Xia T, Li N, Nel AE. Potential health impact of nanoparticles. Annu Rev Public Health. 2009;30:137–50.
78. Nel A, Xia T, Mädler L, Li N. Toxic potential of materials at the nanolevel. Science. 2006;311:622–7.
79. Nel AE, Mädler L, Velegol D, Xia T, Hoek EM, Somasundaran P, Klaessig F, Castranova V, Thompson M. Understanding biophysicochemical interactions at the nano-bio interface. Nat Mater. 2009;8:543–57.
80. Soenen SJ, Nuytten N, De Meyer SF, De Smedt SC, De Cuyper M. High intracellular iron oxide nanoparticle concentrations affect cellular cytoskeleton and focal adhesion kinase-mediated signaling. Small. 2010;6:832–42.
81. Singh N, Manshian B, Jenkins GJ, Griffiths SM, Williams PM, Maffeis TG, Wright CJ, Doak SH. NanoGenotoxicology: the DNA damaging potential of engineered nanomaterials. Biomaterials. 2009;30:3891–914.
82. Ramírez-García G, Gutiérrez-Granados S, Gallegos-Corona MA, Palma-Tirado L, d'Orlyé F, Varenne A, Mignet N, Richard C, Martínez-Alfaro M. Long-term toxicological effects of persistent luminescence nanoparticles after intravenous injection in mice. Int J Pharm. 2017;532:686–95.
83. Li J, Shi J, Shen J, Man H, Wang M, Zhang H. Specific recognition of breast cancer cells in vitro using near infrared-emitting long-persistence luminescent Zn(3)Ga(2)Ge(2)O(10):Cr(3+) nanoprobes. Nano-Micro Lett. 2015;7:138–45.
84. Maldiney T, Kaikkonen MU, Seguin J, le Masne de Chermont Q, Bessodes M, Airenne KJ, Ylä-Herttuala S, Scherman D, Richard C. In vitro targeting of avidin-expressing glioma cells with biotinylated persistent luminescence nanoparticles. Bioconjug Chem. 2012;23:472–8.
85. Zhang HJ, Zhao X, Chen LJ, Yang CX, Yan XP. Dendrimer grafted persistent luminescent nanoplatform for aptamer guided tumor imaging and acid-responsive drug delivery. Talanta. 2020;219:121209.
86. Yan Z, Wang Y, Qiu M, Long K, Zhang Z, Sun M, Yin C, Wang W, Wang HQ, Yuan Z. Persistent luminescence nanoparticles with high intensity for colorectal cancer surgery navigation and precision resection. J Mater Chem B. 2024;12:8655–61.
87. Su YB, Zhao X, Chen LJ, Qian HL, Yan XP. Fabrication of G-quadruplex/porphyrin conjugated gold/persistent luminescence theranostic nanoprobe for imaging-guided photodynamic therapy. Talanta. 2021;233:122567.
88. Cui M, Dai P, Ding J, Li M, Sun R, Jiang X, Wu M, Pang X, Liu M, Zhao Q, et al. Millisecond-range time-resolved bioimaging enabled through ultralong aqueous phosphorescence probes. Angew Chem, Int Ed Engl. 2022;61:e202200172.
89. Zhao HX, Yang CX, Yan XP. Fabrication and bioconjugation of B(III) and Cr(III) co-doped ZnGa(2)O(4) persistent luminescent nanoparticles for dual-targeted cancer bioimaging. Nanoscale. 2016;8:18987–94.
90. Lyu Y, Cui D, Huang J, Fan W, Miao Y, Pu K. Near-infrared afterglow semiconducting nano-polycomplexes for the multiplex differentiation of cancer exosomes. Angew Chem Int Ed Engl. 2019;58:4983–7.
91. Wu L, Ishigaki Y, Hu Y, Sugimoto K, Zeng W, Harimoto T, Sun Y, He J, Suzuki T, Jiang X, et al. H(2)S-activatable near-infrared afterglow

luminescent probes for sensitive molecular imaging in vivo. Nat Commun. 2020;11:446.
92. Tan J, Li H, Ji C, Zhang L, Zhao C, Tang L, Zhang C, Sun Z, Tan W, Yuan Q. Electron transfer-triggered imaging of EGFR signaling activity. Nat Commun. 2022;13:594.
93. Liu N, Shi J, Wang Q, Guo J, Hou Z, Su X, Zhang H, Sun X. In vivo repeatedly activated persistent luminescence nanoparticles by radiopharmaceuticals for long-lasting tumor optical imaging. Small. 2020;16:e2001494.
94. Wang Y, Li Z, Lin Q, Wei Y, Wang J, Li Y, Yang R, Yuan Q. Highly sensitive detection of bladder cancer-related miRNA in urine using time-gated luminescent biochip. ACS Sens. 2019;4:2124–30.
95. Wu BY, Yan XP. Bioconjugated persistent luminescence nanoparticles for Föster resonance energy transfer immunoassay of prostate specific antigen in serum and cell extracts without in situ excitation. Chem Commun. 2015;51:3903–6.
96. Jain PK, Lee KS, El-Sayed IH, El-Sayed MA. Calculated absorption and scattering properties of gold nanoparticles of different size, shape, and composition: applications in biological imaging and biomedicine. J Phys Chem B. 2006;110:7238–48.
97. Liu J, Kotrchova L, Lecuyer T, Corvis Y, Seguin J, Mignet N, Etrych T, Scherman D, Randarova E, Richard C. Coating persistent luminescence nanoparticles with hydrophilic polymers for in vivo imaging. Front Chem. 2020;8:584114.
98. Algar WR, Massey M, Rees K, Higgins R, Krause KD, Darwish GH, Peveler WJ, Xiao Z, Tsai HY, Gupta R, et al. Photoluminescent nanoparticles for chemical and biological analysis and imaging. Chem Rev. 2021;121:9243–358.
99. O'Shannessy DJ, Somers EB, Maltzman J, Smale R, Fu YS. Folate receptor alpha (FRA) expression in breast cancer: identification of a new molecular subtype and association with triple negative disease. Springerplus. 2012;1:22.
100. Boogerd LS, Boonstra MC, Beck AJ, Charehbili A, Hoogstins CE, Prevoo HA, Singhal S, Low PS, van de Velde CJ, Vahrmeijer AL. Concordance of folate receptor-α expression between biopsy, primary tumor and metastasis in breast cancer and lung cancer patients. Oncotarget. 2016;7:17442–54.
101. Chen LJ, Sun SK, Wang Y, Yang CX, Wu SQ, Yan XP. Activatable multifunctional persistent luminescence nanoparticle/copper sulfide nanoprobe for in vivo luminescence imaging-guided photothermal therapy. ACS Appl Mater Interfaces. 2016;8:32667–74.
102. Chen W, Zhang J. Using nanoparticles to enable simultaneous radiation and photodynamic therapies for cancer treatment. J Nanosci Nanotechnol. 2006;6:1159–66.
103. Li X, Lee D, Huang JD, Yoon J. Phthalocyanine-assembled nanodots as photosensitizers for highly efficient type i photoreactions in photodynamic therapy. Angew Chem Int Ed Engl. 2018;57:9885–90.
104. Sun SK, Wu JC, Wang H, Zhou L, Zhang C, Cheng R, Kan D, Zhang X, Yu C. Turning solid into gel for high-efficient persistent luminescence-sensitized photodynamic therapy. Biomaterials. 2019;218:119328.
105. Fujishiro R, Sonoyama H, Ide Y, Fujimura T, Sasai R, Nagai A, Mori S, Kaufman NEM, Zhou Z, Vicente MGH, et al. Synthesis, photodynamic activities, and cytotoxicity of new water-soluble cationic gallium(III) and zinc(II) phthalocyanines. J Inorg Biochem. 2019;192:7–16.
106. Abdurahman R, Yang CX, Yan XP. Conjugation of a photosensitizer to near infrared light renewable persistent luminescence nanoparticles for photodynamic therapy. Chem Commun (Camb). 2016;52:13303–6.
107. Fan W, Lu N, Xu C, Liu Y, Lin J, Wang S, Shen Z, Yang Z, Qu J, Wang T, et al. Enhanced afterglow performance of persistent luminescence implants for efficient repeatable photodynamic therapy. ACS Nano. 2017;11:5864–72.
108. Chen H, Zheng B, Liang C, Zhao L, Zhang Y, Pan H, Ji W, Gong X, Wang H, Chang J. Near-infrared persistent luminescence phosphors ZnGa(2)O(4):Cr(3+) as an accurately tracker to photothermal therapy in vivo for visual treatment. Mater Sci Eng C Mater Biol Appl. 2017;79:372–81.
109. Cheng C-L, Chan M-H, Feng S-J, Hsiao M, Liu R-S. Long-term near-infrared signal tracking of the therapeutic changes of glioblastoma cells in brain tissue with ultrasound-guided persistent luminescent nanocomposites. ACS Appl Mater Interfaces. 2021;13:6099–108.
110. Zhao X, Zhao KC, Chen LJ, Liu YS, Liu JL, Yan XP. A pH reversibly activatable NIR photothermal/photodynamic-in-one agent integrated with renewable nanoimplants for image-guided precision phototherapy. Chem Sci. 2020;12:442–52.
111. Stewart HL, Birch DJS. Fluorescence guided surgery. Methods Appl Fluoresc. 2021;9:1088.
112. Sutton PA, van Dam MA, Cahill RA, Mieog S, Polom K, Vahrmeijer AL, van der Vorst J. Fluorescence-guided surgery: comprehensive review. BJS Open. 2023;7:49.
113. Thammineedi SR, Saksena AR, Nusrath S, Iyer RR, Shukla S, Patnaik SC, Reddy RP, Boleneni N, Sharma RM, Smith L, et al. Fluorescence-guided cancer surgery—a new paradigm. J Surg Oncol. 2021;123:1679–98.
114. Liu J, Lécuyer T, Seguin J, Mignet N, Scherman D, Viana B, Richard C. Imaging and therapeutic applications of persistent luminescence nanomaterials. Adv Drug Deliv Rev. 2019;138:193–210.
115. Lécuyer T, Teston E, Ramirez-Garcia G, Maldiney T, Viana B, Seguin J, Mignet N, Scherman D, Richard C. Chemically engineered persistent luminescence nanoprobes for bioimaging. Theranostics. 2016;6:2488–524.
116. Sun SK, Wang HF, Yan XP. Engineering persistent luminescence nanoparticles for biological applications: from biosensing/bioimaging to theranostics. Acc Chem Res. 2018;51:1131–43.
117. Ni X, Zhang X, Duan X, Zheng HL, Xue XS, Ding D. Near-infrared afterglow luminescent aggregation-induced emission dots with ultrahigh tumor-to-liver signal ratio for promoted image-guided cancer surgery. Nano Lett. 2019;19:318–30.
118. Ai T, Shang W, Yan H, Zeng C, Wang K, Gao Y, Guan T, Fang C, Tian J. Near infrared-emitting persistent luminescent nanoparticles for hepatocellular carcinoma imaging and luminescence-guided surgery. Biomaterials. 2018;167:216–25.
119. Lin P, Shi J, Lin Y, Zhang Q, Yu K, Liu L, Song L, Kang Y, Hong M, Zhang Y. Near-infrared persistent luminescence nanoprobe for ultrasensitive image-guided tumor resection. Adv Sci (Weinheim, Ger). 2023;10:e2207486.
120. Gu J, Zhang H, Hu M, Liu L, Chen C, Wang J, Zhu F, Wei G, Huo J. Complementary and alternative medicine in relation to chemotherapy-induced peripheral neuropathy: a narrative review. Explore-J Sci Heal. 2024;20:181–7.
121. Chen LJ, Yang CX, Yan XP. Liposome-coated persistent luminescence nanoparticles as luminescence trackable drug carrier for chemotherapy. Anal Chem. 2017;89:6936–9.
122. Maldiney T, Ballet B, Bessodes M, Scherman D, Richard C. Mesoporous persistent nanophosphors for in vivo optical bioimaging and drug-delivery. Nanoscale. 2014;6:13970–6.
123. Zhang HJ, Zhao X, Chen LJ, Yang CX, Yan XP. pH-driven targeting nanoprobe with dual-responsive drug release for persistent luminescence imaging and chemotherapy of tumor. Anal Chem. 2020;92:1179–88.
124. Wang ZH, Liu JM, Li CY, Wang D, Lv H, Lv SW, Zhao N, Ma H, Wang S. Bacterial biofilm bioinspired persistent luminescence nanoparticles with gut-oriented drug delivery for colorectal cancer imaging and chemotherapy. ACS Appl Mater Interfaces. 2019;11:36409–19.
125. Chen H, Sun X, Wang GD, Nagata K, Hao Z, Wang A, Li Z, Xie J, Shen B. LiGa5O8:Cr-based theranostic nanoparticles for imaging-guided X-ray induced photodynamic therapy of deep-seated tumors. Mater Horiz. 2017;4:1092–101.
126. Shi J, Sun X, Zheng S, Song L, Zhang F, Madl T, Zhang Y, Zhang H, Hong M. Tin-doped near-infrared persistent luminescence nanoparticles with considerable improvement of biological window activation for deep tumor photodynamic therapy. ACS Appl Bio Mater. 2020;3:5995–6004.
127. Su F-X, Zhao X, Dai C, Li Y-J, Yang C-X, Yan X-P. A multifunctional persistent luminescent nanoprobe for imaging guided dual-stimulus responsive and triple-synergistic therapy of drug resistant tumor cells. Chem Commun. 2019;55:5283–6.
128. Zou R, Li J, Yang T, Zhang Y, Jiao J, Wong KL, Wang J. Biodegradable manganese engineered nanocapsules for tumor-sensitive near-infrared persistent luminescence/magnetic resonance imaging and simultaneous chemotherapy. Theranostics. 2021;11:8448–63.
129. Yang L, Gai SL, Ding H, Yang D, Feng LL, Yang pp. Recent progress in inorganic afterglow materials: mechanisms, persistent luminescent properties, modulating methods, and bioimaging applications. Adv Opt Mater. 2023;11:43.
130. Chen X, Li Y, Huang K, Huang L, Tian X, Dong H, Kang R, Hu Y, Nie J, Qiu J, et al. Trap energy upconversion-like near-infrared to

near-infrared light rejuvenateable persistent luminescence. Adv Mater. 2021;33:e2008722.
131. Liu YQ, Qin LY, Li HJ, Wang YX, Zhang R, Shi JM, Wu JH, Dong GX, Zhou P. Application of lanthanide-doped upconversion nanoparticles for cancer treatment: a review. Nanomedicine (Lond). 2021;16:2207–42.
132. Feng Y, Chen H, Wu Y, Que I, Tamburini F, Baldazzi F, Chang Y, Zhang H. Optical imaging and pH-awakening therapy of deep tissue cancer based on specific upconversion nanophotosensitizers. Biomaterials. 2020;230:119637.
133. Wu S, Li Y, Zhang R, Fan K, Ding W, Xu L, Zhang L. Persistent luminescence-polypyrrole nanocomposite for dual-modal imaging and photothermal therapy of mammary cancer. Talanta. 2021;221:121435.

Publisher's Note